# Synthesis, Structural Studies, and Oxidation Catalysis of the Late-First-Row-Transition-Metal Complexes of a 2-Pyridylmethyl Pendant-Armed Ethylene Cross-Bridged Cyclam

Donald G. Jones,[†] Kevin R. Wilson,[†] Desiray J. Cannon-Smith,[†] Anthony D. Shircliff,[†] Zhan Zhang,[‡] Zhuqi Chen,[‡] Timothy J. Prior,*[,§] Guochuan Yin,*[,‡] and Timothy J. Hubin*[,†]

[†]Department of Chemistry and Physics, Southwestern Oklahoma State University, 100 Campus Drive, Weatherford, Oklahoma 73096, United States

[‡]Key Laboratory for Large-Format Battery Materials and System, Ministry of Education, School of Chemistry and Chemical Engineering, Hubei Key Laboratory of Material Chemistry and Service Failure, Huazhong University of Science and Technology, Wuhan 430074, P. R. China

[§]Department of Chemistry, The University of Hull, Cottingham Road, Hull HU6 7RX, U.K.

Ⓢ *Supporting Information*

**ABSTRACT:** The first 2-pyridylmethyl pendant-armed ethylene cross-bridged cyclam ligand has been synthesized and successfully complexed to $Mn^{2+}$, $Fe^{2+}$, $Co^{2+}$, $Ni^{2+}$, $Cu^{2+}$, and $Zn^{2+}$ cations. X-ray crystal structures were obtained for all six complexes and demonstrate pentadentate binding of the ligand with the requisite cis-V configuration of the cross-bridged cyclam ring in all cases, leaving a potential labile binding site cis to the pyridine donor for interaction of the complex with oxidants and/or substrates. The electronic properties of the complexes were evaluated using solid-state magnetic moment determination and acetonitrile solution electronic spectroscopy, which both agree with the crystal structure determination of high-spin divalent metal complexes in all cases. Cyclic voltammetry in acetonitrile revealed reversible redox processes in all but the $Ni^{2+}$ complex, suggesting that catalytic reactivity involving electron-transfer processes is possible for complexes of this ligand. Kinetic studies of the dissociation of the ligand from the copper(II) complex under strongly acidic conditions and elevated temperatures revealed that the pyridine pendant arm actually destabilizes the complex compared to the parent cross-bridged cyclam complex. Screening for oxidation catalysis using hydrogen peroxide as the terminal oxidant for the most biologically relevant $Mn^{2+}$, $Fe^{2+}$, and $Cu^{2+}$ complexes identified the $Mn^{2+}$ complex as a potential mild oxidation catalyst worthy of continued development.
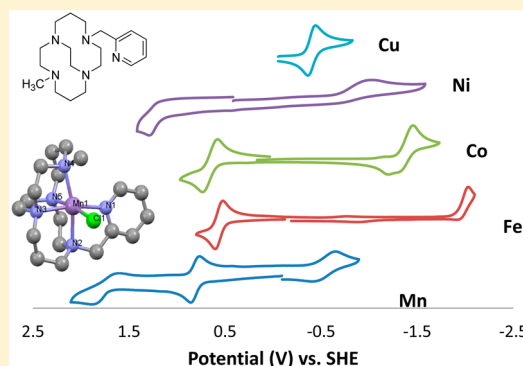
## INTRODUCTION

Oxidation catalysis by cross-bridged cyclam complexes of manganese and iron has been studied for nearly a decade and a half.[1−14] The manganese complex of 4,11-dimethyl-1,4,8,11-tetraazabicyclo[6.6.2]hexadecane[15] (**Me₂EBC**, Scheme 1) in particular has a diverse and rich oxidation chemistry utilizing oxidation mechanisms ranging from hydrogen-atom abstraction (HAT), electron transfer, concerted oxygen-atom transfer (OAT), to the oxygen-rebound mechanism.[5−14] This compound, which we propose to call "the Busch catalyst", was initially targeted as a potential oxidation catalyst because the rigid cross-bridged ligand could strongly bind the oxygen-reactive manganese ion and prevent it from being deactivated in the form of $MnO_2$.[1−4] Additional critical ligand properties are thought to be the two available cis labile coordination sites for oxidant and substrate interaction, the methyl groups sterically preventing dimerization, which might deactivate the catalyst, and the saturated and all-tertiary nitrogen nature of the ligand, which minimizes the possibility of ligand oxidation and catalyst

destruction.[1−4] Mn(**Me₂EBC**)Cl₂ is a patented bleach catalyst heavily invested in by the laundry detergent industry because of its ability to activate $O_2/H_2O_2$ in water and remove stain molecules from cloth.[16−20] However, it has not been fully implemented in consumer products.

Recently, Que and co-workers have revisited the iron complex of **Me₂EBC** and observed efficient olefin epoxidation catalysis with hydrogen peroxide (H₂O₂) oxidant under appropriate conditions.[21] In this study, it was shown that added acetic acid increases the yield of the epoxide product, and it was postulated that acetic acid binds to the iron center and facilitates O−O bond cleavage, which is dependent on the cis orientation of the two labile sites. Only one ligand-modified analogue of **Me₂EBC**, the diethyl analogue **Et₂EBC** (Scheme 1), has had its manganese complex oxidation catalysis explored.[22,23] Interestingly, the seemingly simple exchange of

**Scheme 1. Ligands Discussed in This Paper**



Me₂EBC          TMC-py          PyMeEBC



Et₂EBC
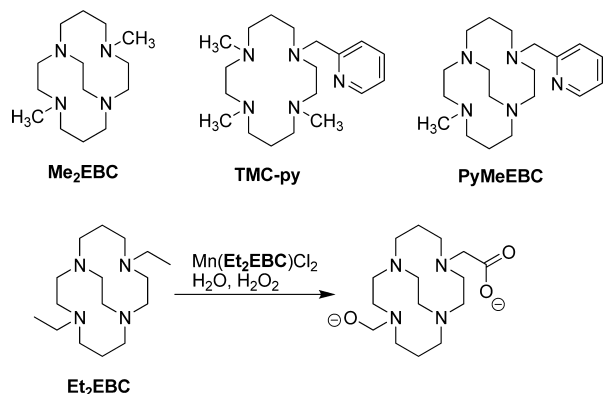
methyl for ethyl groups results in a large change in the catalyst oxidation potential and the surprising oxidation of the two ethyl groups into chelated methylene carboxylato and ethoxo groups (Scheme 1), respectively. While demonstrating the large possible effect of modifying the **Me₂EBC** ligand structure on the oxidation potential and thus the resulting catalytic behavior, the hexadentate-modified ligand product reduces the utility of the ultimate product in this case by coordinatively saturating it. Additional motivation derived from (trimethylpyridyl)cyclam (**TMC-py**, Scheme 1), having all but the desired ethylene cross-bridge of our preferred ligand characteristics (vide supra). Its iron complex activated dioxygen and formed an oxoiron(IV) intermediate, which was crystallographically characterized but has not been pursued further as a catalyst.[24] Although other pyridyl pendant-armed unbridged cyclams are ubiquitous[25−35] and a dipyridyl pendant-armed cross-bridged cyclen has been published,[36] none of these ligands provide all of the desirable features for an oxidation catalyst (vide supra).

In this report, we offer our initial contribution to this field with the synthesis and characterization of a 2-pyridylmethyl N-pendant arm ethylene cross-bridged cyclam (**PyMeEBC**, Scheme 1) and its late-first-row-transition-metal (Mn²⁺, Fe²⁺, Co²⁺, Ni²⁺, Cu²⁺, and Zn²⁺) complexes. We chose to modify **Me₂EBC** by replacing only one methyl with a single 2-pyridylmethyl pendant arm, in order to maintain a labile nonchelated coordination site for interaction with oxidant/substrate. The additional aromatic nitrogen donor was expected to modify the steric and electronic properties of the metal ion, potentially as profoundly as the ethyl groups in **Et₂EBC**,[22,23] resulting in modified oxidation chemistry. The pyridine pendant would also maintain ligand neutrality and steric prevention of dimerization. It was, furthermore, expected that the quaternary, aromatic β-carbon of the pyridyl pendant arm would limit the reactivity of the ligand toward the oxidative modification found in **Et₂EBC**. Here, we disclose its synthesis, complexation to a range of late transition metals, the X-ray crystal structures of all six complexes, their electronic structure as revealed by magnetic moment, UV−vis spectroscopy, and cyclic voltammetry, and the initial screening of the most biomimetically relevant complexes (manganese, iron, and copper) for the ability to catalyze oxidation reactions.

Important results and discussion include the following: (1) synthesis of the first cross-bridged cyclam to include a pendant arm 2-pyridylmethyl group, which will no doubt be exploited by many other coordination chemists for a variety of purposes; (2) X-ray crystal structure characterization of a full series of first-row transition-metal complexes from manganese through zinc

in the same ligand, giving an opportunity to examine coordination preference, and geometric and parametric changes as the size and electronic properties change throughout the series; (3) the effect of an added pyridine donor on the electronic properties of the resulting complexes, most dramatically seen in the increased range of oxidation states available and increased reversibility observed in the cyclic voltammetry; (4) oxidation screening through HAT and OAT reactions that identify the Mn(**PyMeEBC**)Cl⁺ complex as an active oxidation catalyst that may have significant advantages over Mn(**Me₂EBC**)Cl₂ as a laundry bleach catalyst due to enhanced oxidation selectivity; (5) kinetic decomplexation studies of the Cu(**PyMeEBC**)²⁺ complex that in comparison with literature data indicate that the pyridine pendant arm actually destabilizes the complex with respect to the parent **Me₂EBC** ligand, even though an additional chelate ring is added.

## ■ EXPERIMENTAL SECTION

**General Procedures.** N,N′-Bis(aminopropyl)ethylenediamine (98%) and 2-picolyl chloride hydrochloride (98%) were purchased from Acros Organics. Glyoxal (40 wt % in water), methyl iodide (99%), and sodium borohydride (NaBH₄; 98%), all anhydrous divalent transition-metal chloride salts, and all anhydrous solvents used in the glovebox were purchased from Aldrich Chemical Co. All other solvents were of reagent grade and were used without modification. Cyclam was prepared according to a modified literature method from N,N′-bis(aminopropyl)ethylenediamine.[37] cis-3a,5a,8a,10a-Tetraazaperhydropyrene (**1**, cyclam glyoxal) was prepared according to a literature method.[38] Elemental analyses were performed by Quantitative Technologies Inc. Electrospray mass spectra were collected on a Shimadzu LCMS-2020 instrument. All samples were dissolved in 50% water (H₂O)/50% methanol (MeOH). NMR spectra were obtained on a Varian Bruker AVANCE II 300 MHz NMR spectrometer. Electronic spectra were recorded using a Shimadzu UV-3600 UV−vis−near-IR spectrophotometer. Magnetic moments were obtained on finely ground solid samples at ambient temperatures using a Johnson Matthey MSB Auto magnetic susceptibility balance.

**Electrochemistry.** Electrochemical experiments were performed on a BAS Epsilon EC-USB electrochemical analyzer. A button platinum electrode was used as the working electrode with a platinum wire counter electrode and a silver wire pseudoreference electrode. Scans were taken at 200 mV/s. Acetonitrile solutions of the complexes (1 mM) with tetrabutylammonium hexafluorophosphate (0.1 M) as the supporting electrolyte were used. The measured potentials were referenced to SHE using ferrocene (+0.400 V versus SHE) as an internal standard. All electrochemical measurements were carried out under nitrogen.

**Acid Decomplexation Studies.** [Cu(**Me₂EBC**)Cl]PF₆ synthesized according to the literature[39] and [Cu(**PyMeEBC**)][PF₆]₂ synthesized as below were used at 1 mM. The complex's lone d−d absorption was recorded on a Shimadzu UV-3600 UV−vis−near-IR spectrophotometer in 5 M HCl at both 90 and 50 °C over time. Typically, isosbestic spectra indicated only one decomposition product as the absorbance at λ_max decreased over time. Pseudo-first-order conditions allowed the calculation of half-lives from the slopes of the linear ln(absorbance) versus time plots.

**Synthesis.** *3a-(Pyridin-2-ylmethyl)decahydro-5a,8a,10a-triaaza-3a-azoniapyrenium Iodide (2).* A total of 13.28 g (0.08096 mol, 2 equiv) of picolyl chloride hydrochloride and 13.60 g (0.1619 mol, 4 equiv) of anhydrous NaHCO₃ were stirred in 700 mL of chloroform for 1 h. Solids were removed by filtration, and the filtrate was added to 9.00 g (0.04048 mol, 1 equiv) of **1** and 13.44 g (0.08096 mol, 2 equiv) of KI. The reaction was stirred and heated to reflux for 6 days under nitrogen, during which it became an orange color. After cooling, minimal solids were removed by filtration and discarded. The filtrate was evaporated to 100 mL volume, and excess diethyl ether was added to precipitate the yellow solid product, which was filtered on a glass

frit, washed with diethyl ether, and dried under vacuum. Yield: 11.841 g (66%). Electrospray mass spectrometry gave a single peak at $m/z$ 314 corresponding to $(M − I)^+$. Anal. Calcd for $C_{18}H_{28}N_5I \cdot H_2O$: C, 47.06; H, 6.58; N, 15.25. Found: C, 46.87; H, 6.54; N, 14.88. $^1H$ NMR (300 MHz, $CDCl_3$): δ 1.36 (d, 1H), 1.84 (d, 1H), 2.25 (m, 2H), 2.41 (d, 1H), 2.56 (d, 1H), 2.66 (m, 2H), 3.03 (m, 6H), 3.23 (t, 1H), 3.65 (m, 2H), 3.89 (d, 1H), 4.21 (m, 2H), 4.40 (td, 1H), 4.58 (s, 1H), 5.45 (m, 2H), 7.41 (m, 1H), 7.84 (m, 1H), 8.31 (d, 1H), 8.66 (d, 1H). $^{13}C\{^1H\}$ NMR (75.6 MHz, $D_2O$): δ 18.0, 18.4, 41.9, 46.6, 49.4, 51.3, 51.9, 53.2, 54.0, 60.5, 62.9, 69.5, 82.2, 125.8, 129.0, 138.6, 146.6, 150.3.

*3a-(Pyridin-2-ylmethyl)-8a-methyldecahydro-5a,10a-diaaza-3a,8a-diazoniapyrenium Diiodide (3).* A total of 11.841 g (0.02683 mol, 1 equiv) of **2** was suspended in 690 mL of dry acetonitrile in a 1 L round-bottomed flask. A total of 15 equiv (0.4025 mol, 57.13 g, 25.17 mL) of iodomethane was added, the flask was stoppered, and the reaction was stirred at room temperature for 7 days. The light-brown solid product was obtained by filtration on a glass frit, washing with diethyl ether, and drying under vacuum. A second crop was obtained by the addition of excess ether to the filtrate and added to the first crop. Yield: 12.921 g (83%). Electrospray mass spectrometry gave peaks at $m/z$ 456 corresponding to $(M − I)^+$, $m/z$ 328 corresponding to $(M − 2I)^+$, and $m/z$ 165 corresponding to $(M − 2I)^{2+}$. Anal. Calcd for $C_{19}H_{31}N_5I_2 \cdot 0.5CH_3CN$: C, 39.78; H, 5.43; N, 12.76. Found: C, 39.51; H, 5.63; N, 13.09. $^1H$ NMR (300 MHz, $CDCl_3$): δ 1.80 (m, 2H), 1.97 (s, 3H), 2.32 (m, 3H), 2.79 (td, 1H), 3.10 (m, 5H), 3.38 (m, 5H), 3.55 (d, 2H), 3.72 (d, 2H), 4.51 (m, 2H), 5.18 (d, 2H), 7.52 (m, 1H), 7.65 (d, 1H), 7.93 (m, 1H), 8.65 (d, 1H). $^{13}C\{^1H\}$ NMR (75.6 MHz, $D_2O$): δ 17.1, 17.5, 45.3, 45.6, 47.4, 48.4, 48.7, 49.8, 50.2, 59.6, 62.0, 64.1, 73.6, 75.7, 125.0, 128.2, 137.7, 145.3, 149.5.

*4-Methyl-11-(pyridin-2-ylmethyl)-1,4,8,11-tetraazabicyclo[6.6.2]-hexadecane (**PyMeEBC**).* A total of 9.010 g (0.0154 mol, 1 equiv) of **3** was dissolved in 550 mL of 95% ethanol (EtOH). A total of 8.739 g (0.2310 mol, 15 equiv) of $NaBH_4$ was added over 5 min. The reaction was then stirred under nitrogen for 5 days; copious white precipitate formed during the course of the reaction. Excess $NaBH_4$ was decomposed by the slow addition of concentrated HCl. EtOH was removed under vacuum, after which 500 mL of 30% aqueous KOH was added. This basic solution was extracted with five 200 mL portions of benzene. The combined benzene layers were dried over sodium sulfate, filtered, and evaporated to a pale-yellow oil, which was not purified further. Yield: 4.550 g (89%). Electrospray mass spectrometry gave a single peak at $m/z$ 332 corresponding to $(MH)^+$. Anal. Calcd for $C_{19}H_{33}N_5 \cdot 0.3H_2O \cdot 0.1C_6H_6$: C, 68.29; H, 10.00; N, 20.32. Found: C, 68.40; H, 10.52; N, 20.33. $^1H$ NMR (300 MHz, $CDCl_3$): δ 1.68 (m, 4H), 2.30 (s, 3H), 2.85 (m, 18H), 3.58 (m, 4H), 7.16 (m, 2H), 7.61 (m, 1H), 8.49 (m, 1H). $^{13}C\{^1H\}$ NMR (75.6 MHz, $CDCl_3$): δ 22.9, 23.6, 41.5, 50.3, 50.6, 51.3, 51.8, 52.2, 52.8, 53.3, 55.7, 56.8, 57.6, 58.6, 122.0, 123.1, 135.6, 148.4, 156.1.

**[Mn(PyMeEBC)Cl]Cl.** A total of 1.000 g (0.003017 mol) of **PyMeEBC** and 0.380 g (0.003016 mol) anhydrous $MnCl_2$ were added to 20 mL of anhydrous acetonitrile in an inert-atmosphere glovebox. The reaction was stirred at room temperature for 2 days, during which the pink $MnCl_2$ beads dissolved and the white precipitate powder product precipitated. This product was obtained by filtration on a glass frit, washed with ether, and allowed to dry open to the atmosphere of the glovebox for 4 days. Yield: 0.930 g (67%). Electrospray mass spectrometry gave peaks at $m/z$ 421 corresponding to $(Mn-(PyMeEBC)Cl)^+$ and $m/z$ 193 corresponding to $(Mn(PyMeEBC))^{2+}$. Anal. Calcd for $[Mn(C_{19}H_{33}N_5)Cl]Cl \cdot 0.1H_2O$: C, 49.70; H, 7.29; N, 15.25. Found: C, 49.35; H, 7.21; N, 15.09.

**[M(PyMeEBC)Cl]PF₆** where M = $Mn^{2+}$, $Fe^{2+}$, $Co^{2+}$, $Ni^{2+}$, and $Zn^{2+}$. The general procedure for [Mn(**PyMeEBC**)Cl]Cl was followed using 0.001 mol (0.332 g) of **PyMeEBC** and 0.001 mol of the respective anhydrous divalent metal chloride salt. [Because $NiCl_2$ has little solubility in acetonitrile, *N,N*-dimethylformamide (DMF) was used as the solvent for this reaction only. The reaction was removed from the glovebox and refluxed overnight before workup.] These reactions, other than manganese, gave little or no precipitation. All were filtered to remove trace solids, which were discarded (other than manganese, which gave a copious white solid, which was filtered,

dissolved in a minimum of MeOH, and precipitated with $NH_4PF_6$ as for the other metal ions). The filtrates were then evaporated under vacuum to give crude [M(**PyMeEBC**)Cl]Cl solid products that were dissolved in a minimum of MeOH in the glovebox. To each was added 0.815 g (0.005 mol, 5 equiv) of $NH_4PF_6$, likewise dissolved in a minimum of MeOH. Precipitation of the [M(**PyMeEBC**)Cl]PF₆ products was immediate, but the suspensions were allowed to stir approximately 1 h to complete precipitation. The solid [M-(**PyMeEBC**)Cl]PF₆ products were filtered off, washed with diethyl ether, and allowed to dry overnight open to the glovebox atmosphere.

**[Mn(PyMeEBC)Cl]PF₆.** Yield: 0.302 g (53%) of white powder. Electrospray mass spectrometry gave peaks at $m/z$ 421 corresponding to $(Mn(PyMeEBC)Cl)^+$ and $m/z$ 193 corresponding to $(Mn-(PyMeEBC))^{2+}$. Anal. Calcd for $[Mn(C_{19}H_{33}N_5)Cl]PF_6 \cdot 0.5H_2O$: C, 39.63; H, 5.95; N, 12.16. Found: C, 39.46; H, 6.08; N, 12.16. X-ray-quality crystals were obtained from the slow diffusion of diethyl ether into an acetonitrile solution in the glovebox.

**[Fe(PyMeEBC)Cl]PF₆.** Yield: 0.357 g (58%) of yellow powder. Electrospray mass spectrometry gave peaks at $m/z$ 422 corresponding to $(Fe(PyMeEBC)Cl)^+$ and $m/z$ 194 corresponding to $(Fe-(PyMeEBC))^{2+}$. Anal. Calcd for $[Fe(C_{19}H_{33}N_5)Cl]PF_6 \cdot 0.3NH_4PF_6$: C, 37.01; H, 5.59; N, 12.04. Found: C, 37.10; H, 5.27; N, 12.09. X-ray-quality crystals were obtained from the slow evaporation of a MeOH solution in the glovebox.

**[Co(PyMeEBC)Cl]PF₆.** Yield: 0.401 g (70%) of pink powder. Electrospray mass spectrometry gave peaks at $m/z$ 425 corresponding to $(CoLCl)^+$ and $m/z$ 195 corresponding to $(CoL)^{2+}$. Anal. Calcd for $[Co(C_{19}H_{33}N_5)Cl]PF_6$: C, 39.98; H, 5.83; N, 12.27. Found: C, 39.89; H, 5.54; N, 12.18. X-ray-quality crystals were obtained from the slow diffusion of diethyl ether into an acetonitrile solution in the glovebox.
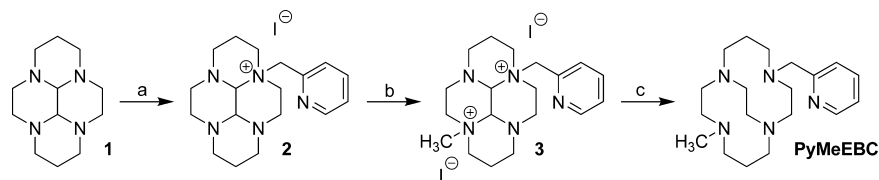
**[Ni(PyMeEBC)Cl]PF₆.** Yield: 0.345 g (60%) of a brown powder. Electrospray mass spectrometry gave peaks at $m/z$ 424 corresponding to $(Ni(PyMeEBC)Cl)^+$, $m/z$ 408 corresponding to $(NiL(H_2O)_2)^+$, and $m/z$ 195 corresponding to $(Ni(PyMeEBC))^{2+}$. Anal. Calcd for $[Ni(C_{19}H_{33}N_5)Cl]PF_6 \cdot 0.2NH_4PF_6 \cdot 1.5H_2O$: C, 36.21; H, 5.89; N, 11.56. Found: C, 36.36; H, 5.61; N, 11.26. X-ray-quality crystals were obtained from the slow diffusion of diethyl ether into a dimethyl sulfoxide solution outside of the glovebox.

**[Zn(PyMeEBC)Cl]PF₆.** Yield: 0.577 g (73%) of a white powder. Electrospray mass spectrometry gave peaks at $m/z$ 430 corresponding to $(Zn(PyMeEBC)Cl)^+$ and $m/z$ 198 corresponding to $(Zn-(PyMeEBC))^{2+}$. Anal. Calcd for $[Zn(C_{19}H_{33}N_5)Cl]PF_6$: C, 39.53; H, 5.76; N, 12.13. Found: C, 39.22; H, 5.49; N, 11.99. X-ray-quality crystals were obtained from the slow evaporation of a nitromethane solution (form 2) and from the slow diffusion of diethyl ether into an acetonitrile solution (form 1), both outside of the glovebox.

**[Cu(PyMeEBC)][PF₆]₂.** This complex was synthesized following the general synthesis of [M(**PyMeEBC**)Cl]PF₆. However, no chloride is bound to the metal ion and two hexafluorophosphate anions are required. Yield: 0.302 g (44%) of a bright blue powder. Electrospray mass spectrometry gave a peak at $m/z$ 197 corresponding to $(Cu(PyMeEBC))^{2+}$. Anal. Calcd for $[Cu(C_{19}H_{33}N_5)][PF_6]_2$: C, 33.32; H, 4.86; N, 10.22. Found C, 32.96; H, 4.65; N, 10.11. X-ray-quality crystals were obtained from the slow diffusion of diethyl ether into an acetonitrile solution outside of the glovebox.

**Crystal Structure Analysis.** Single-crystal X-ray diffraction data were collected in a series of ω scans using a Stoe IPSD2 image-plate diffractometer utilizing monochromated Mo radiation (λ = 0.71073 Å). Standard procedures were employed for integration and processing of the data using *X-RED*.[40] Samples were coated in a thin film of perfluoropolyether oil and mounted at the tip of a glass fiber located on a goniometer. Data were collected from crystals held at 150 K in an Oxford Instruments nitrogen gas cryostream.

Crystal structures were solved using routine automatic direct methods implemented within *SHELXS-97*.[41] Completion of structures was achieved by performing least-squares refinement against all unique $F^2$ values using *SHELXL-97*.[41] All non-hydrogen atoms were refined with anisotropic displacement parameters. Hydrogen atoms were placed using a riding model. Where the location of hydrogen atoms

**Scheme 2. Synthesis of PyMeEBC**[a]



[a](a) (i) CHCl$_3$, 2 equiv of picolyl chloride hydrochloride, 4 equiv of NaHCO$_3$, 1 h, filter to remove solids; (ii) 1 equiv of **1**, 2 equiv of KI, reflux 6 days; 66% yield. (b) CH$_3$CN, 15 equiv of CH$_3$I, 7 days, rt; 83% yield. (c) (i) 95% EtOH, 15 equiv of NaBH$_4$, N$_2$, 5 days, rt; (ii) 12 M HCl(aq), 30% KOH(aq), benzene extraction; 89% yield.

was obvious from difference Fourier maps, C—H bond lengths were refined subject to chemically sensible restraints.

**Catalytic Sulfide Oxidation by Complexes.** In 5 mL of dry acetonitrile containing 0.1 M thioanisole and 0.33 mM complex, 0.2 mL of 30% H$_2$O$_2$ was added to initialize the reaction. The reaction mixture was stirred in a water bath at 303 K for 6 h, and product analysis was performed by gas chromatography (GC) using the internal standard method. A parallel experiment without catalyst was conducted as a control.

**Catalytic HAT by Complexes.** In 3 mL of MeOH/H$_2$O (1:1, v/v) containing 0.05 M 1,4-cyclohexadiene and 1 mM complex, 0.02 mL of 30% H$_2$O$_2$ was added to initialize the reaction. The resulting reaction mixture was stirred in a water bath at 303 K for 4 h, and product analysis was conducted by GC using the internal standard method. A parallel experiment without catalyst was conducted as a control.

## ■ RESULTS AND DISCUSSION

**Synthesis.** Attaching 2-pyridylmethyl N-pendant arms to ethylene cross-bridged tetraazamacrocycles would most efficiently be accomplished by reaction of a halomethylpyridyl moiety with a cyclam—glyoxal bisaminal following the teachings of Weisman et al.[15,42,43] and Handel et al.[38] Initial attempts with picolyl chloride under the typical acetonitrile conditions for such reactions resulted in unsatisfactory red products where the color appeared because of reaction of the picolyl group with itself rather than bisaminal. Literature investigation of the reactivity of halomethylpyridines and halomethylpyrazines led to work where these compounds were stabilized by storage in nonpolar chlorinated solvents.[44] Unsuccessful at alkylation of the bisaminals in typical S$_N$2 solvents like acetonitrile, we explored the chlorinated solvents and found successful, although low-yielding, monoalkylation of the bisaminal **1** with picolyl chloride in chloroform at room temperature. It should be pointed out that others have alkylated cyclam—glyoxal condensates successfully in chloroform, as well.[45] Although we had apparently succeeded in retarding the self-reaction of picolyl chloride because little of the characteristic red color was produced and pure product was obtained, the yields were disappointing at ~10%. We were systematically able to raise the yields through activation of the electrophile by the addition of KI to the reaction, although stoichiometric amounts were required. Additional increases in the temperature (to reflux) and time (to 6 days) eventually led to respectable yields of the monoalkyl salt **2** (66% based on the bisaminal **1**). Again, the uses of I[−46] and heat[45] to increase the reactivity of alkyl agents with macrocycle glyoxal condensates are known strategies. Methylation of the nonadjacent nitrogen to produce **3** and NaBH$_4$ ring-opening reduction to produce **PyMeEBC** successfully followed Weisman et al.'s typical procedures.[15,42,43]

Complexation of **PyMeEBC** was carried out in acetonitrile (or DMF for acetonitrile-insoluble NiCl$_2$) with anhydrous divalent metal salts in an inert-atmosphere glovebox. The white powder manganese complex [Mn(**PyMeEBC**)Cl]Cl precipitated from the reaction and was obtained in pure form by filtration. The other complexes were more soluble, so only trace solids were filtered off, and the solvent was evaporated. The crude chloride salts were not pure, so they were redissolved in MeOH, and the chloride anion was replaced by the addition of NH$_4$PF$_6$ to precipitate the pure [M(**PyMeEBC**)Cl]PF$_6$ powder products. An exception to this formulation was the copper(II) complex, which remained 5-coordinate with no chloro ligand and precipitated as [Cu(**PyMeEBC**)][PF$_6$]$_2$. To aid in crystallization, anion metathesis was similarly achieved to produce [Mn(**PyMeEBC**)Cl]PF$_6$.

Complexation by cross-bridged tetraazamacrocycles is sometimes difficult, requiring heat or long reaction times.[4] Comparatively, complexation with **PyMeEBC** appeared qualitatively to be faster than usual in most cases. For example, a crude [Mn(**PyMeEBC**)Cl]Cl white powder began to precipitate from the room temperature acetonitrile complexation solution within minutes. Similarly, the dramatic color changes indicating Cu$^{2+}$ (dark blue-green) and Co$^{2+}$ (dark purple) coordination with similar ligands were observed immediately upon the addition of metal chloride salts to the room temperature acetonitrile ligand solutions. Therefore, no heat was added to any of the complexation reaction except for NiCl$_2$ complexation, which was done in DMF to aid the solubility of NiCl$_2$, which required heat to fully dissolve this sparingly soluble salt. Certain pendant arms have been noted to aid the speed of complexation of tetraazamacocycles,[47−50] and it is possible that the pyridine pendant arm plays such a role here.

**X-ray Crystal Structures.** *[M(PyMeEBC)Cl]PF$_6$ (M = Mn, Fe, or Co).* The metal(II) complexes [M(**PyMeEBC**)Cl]PF$_6$ (M = Mn, Fe, or Co) are isostructural and crystallize in the noncentrosymmetric space group *Pca*2$_1$. The unit cell volume decreases across this series from manganese to cobalt, in line with reduction in the metal ion radius. The manganese structure is representative of the others, and that one will be discussed in detail to represent the set.

The metal ion lies in an approximately octahedral pocket, coordinated by one chloride anion and five nitrogen atoms from the ligand. The four nitrogen atoms from the macrocycle coordinate to the metal in an "all-cis" arrangement with the pyridyl nitrogen of the pendant arm and the chloride also in a cis arrangement (see Figure 1). This coordination is akin to the cis-V coordination displayed by tetraazamacrocycles bound to a metal bearing two chloride anions.[1,51] Although the four nitrogen atoms of the macrocyle bind to the metal with four- and five-membered chelate rings and N—Mn—N bite angles around 80° and 88°, respectively, the four-membered chelate ring involving the pyridine is noticeably strained, with an N—Mn—N bite angle of 76.79(9)°.
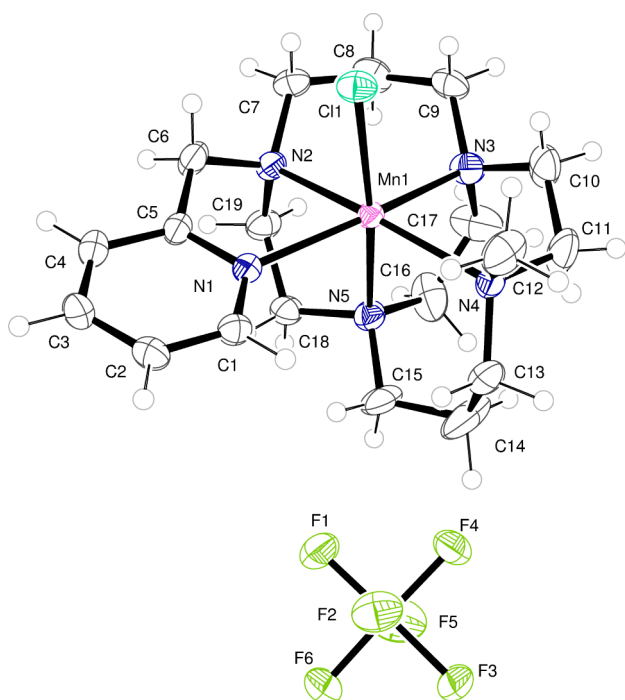
**Figure 1.** Asymmetric unit of $[Mn(\textbf{PyMeEBC})Cl]PF_6$ with atoms drawn as 50% probability ellipsoids. Atom colors: Mn, pink; Cl, green; C, gray; N, blue; F, yellow-green.

*[M(PyMeEBC)Cl]PF$_6$ (M = Ni or Zn).* This macrocycle has also been shown to be a good ligand to smaller metal ions in the complex $[Ni(\textbf{PyMeEBC})Cl]PF_6$ and two different compounds containing the complex ion $[Zn(\textbf{PyMeEBC})Cl]$-$PF_6$, hereafter labeled **Zn-1** (from diffusion of Et$_2$O into a CH$_3$NO$_2$ solution) and **Zn-2** (from evaporation of CH$_3$NO$_2$). The nickel compound is isostructural with **Zn-1**. Therefore, only the nickel compound and not **Zn-1** is described in detail, although the structural discussion applies equally for **Zn-1**.

Although this is centrosymmetric, the asymmetric unit features two symmetry-unique metal complexes, [Ni-

(**PyMeEBC**)Cl]$^+$. They are each 6-coordinate but differ in the arrangement of the alkyl backbone of the ligand.

Figure 2 shows the crystallographic asymmetric unit, and the geometry about each metal ion is further illustrated in Figure 3.
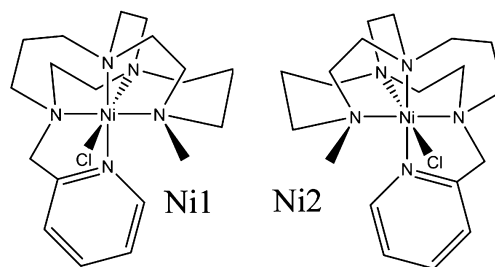


**Figure 3.** Representation of the coordination about the two symmetry-unique metal ions in $[Ni(\textbf{PyMeEBC})Cl]PF_6$.

The coordination about the nickel is completed by one chloride ion and five nitrogen atoms of the ligand. The two symmetry-unique metal ions display the same basic coordination, but they are effectively, although not crystallographically or even parametrically, mirror images. Essentially, the ligand can bind in right- or left-handed orientations, and each is separately present in Ni1 and Ni2. The N–Ni–N bite angles for the pendant pyridyl arm are 81.15(12)° and 81.38(14)° in the two complexes, suggesting a better fit of the Ni$^{2+}$ ion to the macrocycle than for the larger Mn$^{2+}$.

The second polymorph of $[Zn(\textbf{PyMeEBC})Cl]PF_6$ contains a single, octahedrally coordinated Zn$^{2+}$ ion in the asymmetric unit. The zinc ion is bound by five nitrogen atoms of the ligand and one chloride ion, as shown in Figure 4. The coordination geometry is very similar to that of Ni1 in $[Ni(\textbf{PyMeEBC})Cl]$-$PF_6$ (and hence Zn1 in **Zn-1**). The center of inversion within the structure means that the second enantiomer (akin to Ni2) is generated by symmetry.

*[Cu(PyMeEBC)](PF$_6$)$_2$.* The ligand is again found to bind to the metal through each of the five nitrogen atoms, Cu$^{2+}$ is formally 5-coordinate, and no chloride is present in the crystal structure. The geometry about the metal may be described as a
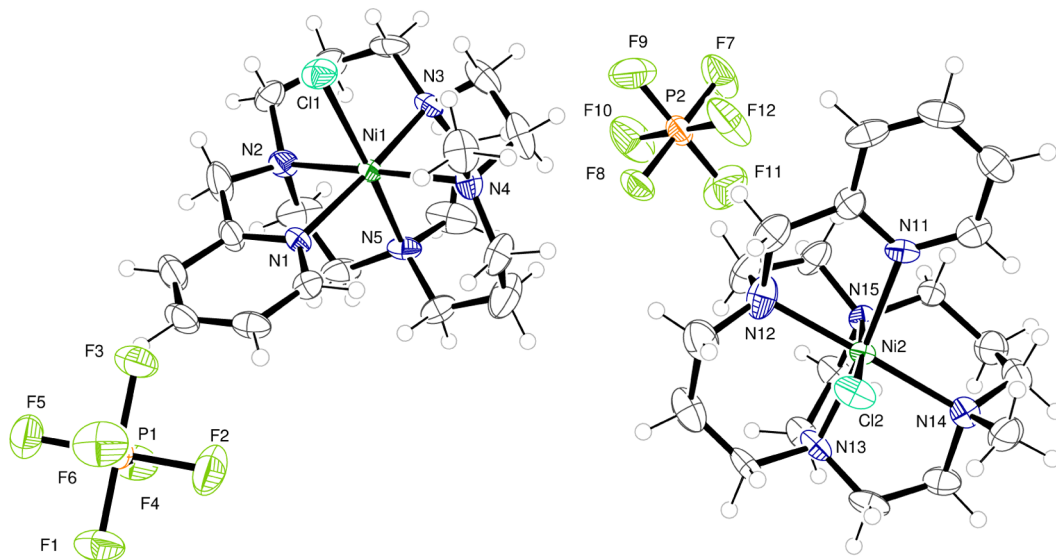


**Figure 2.** ORTEP representation of the asymmetric unit of $[NiLCl]PF_6$ with atoms drawn as 50% probability ellipsoids. Selected atoms are labeled. Atom colors: Ni, deep green; Cl, pale green; C, gray; N, blue; P, orange; F, yellow-green.
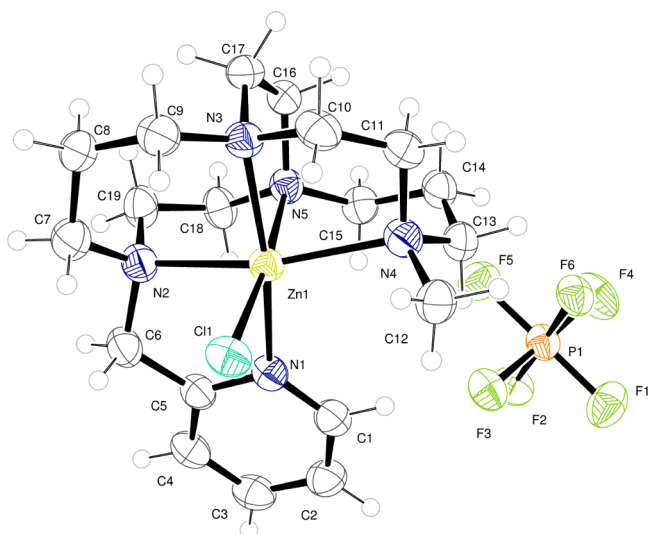
**Figure 4.** ORTEP representation of the asymmetric unit in **Zn-2**, [Zn(**PyMeEBC**)Cl]PF$_6$. Atoms are drawn as 50% probability ellipsoids. Atom colors: Zn, yellow; Cl, pale green; C, gray; N, blue; P, orange; F, yellow-green.

distorted trigonal bipyramid, with N2 and N4 occupying the axial positions and N1, N3, and N5 located in a trigonal plane. The coordination might also be described as a distorted square-based pyramid (N3 as the peak), which highlights the vacant coordination site at the metal (see Figure 5). The Addison parameter[52] ($\tau$) attempts to quantify the degree to which a 5-coordinate structure favors the ideal trigonal-bipyramidal geometry ($\tau$ = 1) or the ideal square-pyramidal geometry ($\tau$ = 0). For this structure, $t$ = 0.48, which indicates that the structure is nearly perfectly intermediate between these two ideals, and thus characterization as either extreme is inadequate.

The charge balancing in this structure is afforded by two PF$_6^-$ anions, one of which forms a close approach to the metal,

such that F12 is near the vacant coordination site at the copper ion and the Cu1···F12 distance is 3.104(3) Å. This is rather longer than the sum of the van der Waals radii[53] of these two ions (2.87 Å), and it is rather longer than the shortest such interactions present in similar systems reported in the Cambridge Structural Database.[54] For a copper ion, coordinated by four or five nitrogen atoms, Cu···F distances of around 2.7 Å are commonly observed, and some much shorter examples are known; e.g., refcode MINKAV has a Cu···F distance of 2.472 Å. It may be the case that this genuinely represents a weak interaction between the Cu$^{2+}$ ion and the fluorine, but the fluorine is not very polarizable, which suggests otherwise. It seems more likely that this close approach facilitates C—H···F interactions between the ligand and PF$_6^-$ anion, i.e., between F12 and H6B, H13B, and H15B and other similar interactions involving the fluorine atoms of this anion.

A final comparison (Table 1) of all of the **PyMeEBC** structures is of interest because all six divalent metal ions from Mn−Zn were coordinated and crystallized in very similar environments. A similar range of metal ions were crystallized in the parent ligand **Me$_2$EBC**,[1,55,39,51,56] and a similar table, although less complete, has appeared previously.[56] In this comparison, the size of the metal ion is correlated to the N$_{ax}$−M−N$_{ax}$ and N$_{eq}$−M−N$_{eq}$ bond angles and generally shows a steady increase in these bond angles as the metal's ionic radius decreases and the bridged macrocycle is better able to engulf the metal ion with less distortion of the expected bond angles. Interestingly, for the larger ions Mn$^{2+}$ and Fe$^{2+}$, the pyridine pendant arm of **PyMeEBC** allows coordination with much less distortion (6−7° larger N$_{ax}$−M−N$_{ax}$ bond angles) than in their complexes with **Me$_2$EBC**. However, this pendent arm effect is not present in the smaller metal ions, or is at least more difficult to discern, because the identities of the nonmacrocyclic ligands are not as directly comparable in some cases.
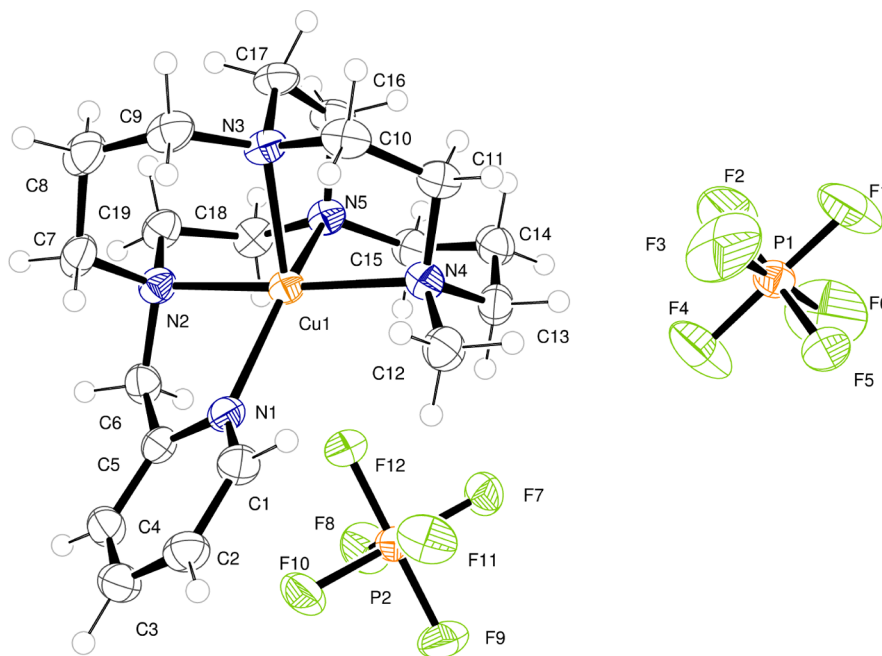


**Figure 5.** ORTEP representation of the asymmetric unit in [Cu(**PyMeEBC**)](PF$_6$)$_2$. Atoms are drawn as 50% probability ellipsoids. Atom colors: Cu, bronze; C, gray; N, blue; P, orange; F, yellow-green.

**Table 1. Comparison of N−M−N Bond Angles for First-Row Divalent Metal Ions with Me$_2$EBC and PyMeEBC from Crystal Structures**[a]

| metal ion | high-spin 6-coordinate ionic radius | Me$_2$EBC | | | | PyMeEBC | |
|---|---|---|---|---|---|---|---|
| | | N$_{ax}$−M−N$_{ax}$ | N$_{eq}$−M−N$_{eq}$ | ref | | N$_{ax}$−M−N$_{ax}$ | N$_{eq}$−M−N$_{eq}$ |
| Mn$^{2+}$ | 97 | 158.0(2) | 75.6(2) | 1 | | 164.74(9) | 78.40(10) |
| Fe$^{2+}$ | 92 | 161.88(5) | 78.36(5) | 1 | | 168.27(8) | 80.82(8) |
| Co$^{2+}$ | 89 | 172.4(2) | 81.11(13) | 51 | | 172.34(12) | 82.88(13) |
| Zn$^{2+}$ | 88 | 171.89(12)[b] | 83.90(11)[b] | 55 | | 168.66 (avg) | 81.84 (avg) |
| Ni$^{2+}$ | 83 | 175.39(5)[c] | 86.16(5)[c] | 56 | | 173.56 (avg) | 84.85 (avg) |
| Ni$^{2+}$ | 83 | 174.56(10)[d] | 85.07(9)[d] | 56 | | | |
| Cu$^{2+}$ | 79[e] | 175.16(13)[e] | 85.30(12)[e] | 39 | | 175.66(13)[e] | 85.24(12)[e] |

[a]Except where noted, all complexes are high-spin 6-coordinate M(**Me$_2$EBC**)Cl$_2$ and M(**PyMeEBC**)Cl$^+$, respectively. [b]Zn(**Me$_2$EBC**)(OAc)(OH$_2$)$^+$. [c]Ni(**Me$_2$EBC**)(OH$_2$)$^{2+}$. [d]Ni(**Me$_2$EBC**)(acac)$^+$. [e]Ionic radius and bond angles are for 5-coordinate complexes.

**Table 2. Crystallographic Data (L = PyMeEBC)**

| | [MnLCl]PF$_6$ sja7_14 DGJ010B | [FeLCl]PF$_6$ sja3_14 DGJ011 | [CoLCl]PF$_6$ sja4_14 DGJ012 | [NiLCl]PF$_6$ sja5_14 DGJ013 | [CuL](PF$_6$)$_2$ sja2_14 DGJ014 | [ZnLCl]PF$_6$ sja1_14b DGJ015 form 1 | [ZnLCl]PF$_6$ sja1_14c DGJ015 form 2 |
|---|---|---|---|---|---|---|---|
| chemical formula | [Mn(C$_{19}$H$_{33}$ N$_5$)Cl]PF$_6$ | [Fe(C$_{19}$H$_{33}$ N$_5$)Cl]PF$_6$ | [Co(C$_{19}$H$_{33}$ N$_5$)Cl]PF$_6$ | [Ni(C$_{19}$H$_{33}$ N$_5$)Cl]PF$_6$ | [Cu(C$_{19}$H$_{33}$ N$_5$)](PF$_6$)$_2$ | [Zn(C$_{19}$H$_{33}$ N$_5$)Cl]PF$_6$ | [Zn(C$_{19}$H$_{33}$ N$_5$)Cl]PF$_6$ |
| $a$ (Å) | 18.5536(10) | 18.5989(9) | 18.6711(13) | 22.758(2) | 10.5546(6) | 22.794(3) | 8.1050(6) |
| $b$ (Å) | 8.6768(4) | 8.6434(6) | 8.6259(10) | 13.730(2) | 13.2043(11) | 13.7535(9) | 22.7534(14) |
| $c$ (Å) | 14.9938(6) | 14.8745(7) | 14.8088(10) | 15.0185(16) | 18.6149(10) | 15.1489(15) | 12.5612(10) |
| $\alpha$ (deg) | 90 | 90 | 90 | 90 | 90 | 90 | 90 |
| $\beta$ (deg) | 90 | 90 | 90 | 93.047(8) | 98.149(5) | 93.512(9) | 97.594(6) |
| $\gamma$ (deg) | 90 | 90 | 90 | 90 | 90 | 90 | 90 |
| $V$ (Å$^3$) | 2413.8(2) | 2391.2(2) | 2385.0(4) | 4686.0(10) | 2568.1(3) | 4740.3(8) | 2296.2(3) |
| $Z$ | 4 | 4 | 4 | 8 | 4 | 8 | 4 |
| fw | 566.86 | 567.77 | 570.85 | 570.62 | 684.98 | 577.29 | 577.29 |
| space group | $Pca2_1$ | $Pca2_1$ | $Pca2_1$ | $P2_1/c$ | $P2_1/c$ | $P2_1/c$ | $P2_1/c$ |
| $T$ (°C) | 150(2) | 150(2) | 150(2) | 150(2) | 150(2) | 150(2) | 150(2) |
| $\lambda$ (Å) | 0.71073 | 0.71073 | 0.71073 | 0.71073 | 0.71073 | 0.71073 | 0.71073 |
| $D_{calcd}$ (g cm$^{-3}$) | 1.560 | 1.577 | 1.590 | 1.618 | 1.772 | 1.618 | 1.670 |
| $\mu$ (mm$^{-1}$) | 0.788 | 0.874 | 0.963 | 1.076 | 1.083 | 1.282 | 1.323 |
| R1($F_o^2$)[a] | 0.0337 | 0.0263 | 0.0329 | 0.0452 | 0.0476 | 0.0504 | 0.0553 |
| wR2 ($F_o^2$)[a] | 0.0848 | 0.0551 | 0.0637 | 0.1062 | 0.1265 | 0.1185 | 0.1451 |

[a]R1 = $\sum ||F_o| - |F_c||/\sum |F_o|$; wR2 = $\{\sum [w(F_o^2 - F_c^2)^2]/\sum [w(F_o^2)^2]\}^{1/2}$.

Crystallographic details for the seven new crystal structures in this work, along with selected bond lengths and angles, are presented in Tables 2 and 3.

**Electronic Structure.** Solid-state magnetic moments were determined for all five paramagnetic **PyMeEBC** complexes. [Mn(**PyMeEBC**)Cl]PF$_6$ gave a magnetic moment of $\mu_{eff}$ = 5.47, which is slightly lower than the expected value (5.65−6.10)[57] but clearly indicative of a high-spin Mn$^{2+}$ d$^5$ ion. The other paramagnetic complexes had magnetic moments within the expected ranges for high-spin divalent metal ions: [Fe(**PyMeEBC**)Cl]PF$_6$, $\mu_{eff}$ = 5.28; [Co(**PyMeEBC**)Cl]PF$_6$, $\mu_{eff}$ = 4.61; [Ni(**PyMeEBC**)Cl]PF$_6$, $\mu_{eff}$ = 2.91; [Cu-(**PyMeEBC**)][PF$_6$]$_2$, $\mu_{eff}$ = 1.79. This high-spin behavior is similar to that of the divalent first-row transition-metal complexes of **Me$_2$EBC**.[1,39,51,56] Apparently, the addition of the pyridine donor, in place of a typically chloro ligand or oxygen donor in the **Me$_2$EBC** complexes, does not cause a change from high spin to low spin, even though pyridine is typically a stronger-field ligand.

Table 4 contains absorbances and extinction coefficients for the six complexes of **PyMeEBC**. The electronic spectra of the zinc complex, with only ligand-based absorbances likely, was obtained to help differentiate these absorbances from the metal-ion-based absorbances of the other complexes. Zn(**PyMeEBC**)-Cl$^+$ had two peaks at 317 nm ($\varepsilon$ = 220 M$^{-1}$ cm$^{-1}$) and 264 nm ($\varepsilon$ = 4120 M$^{-1}$ cm$^{-1}$). The high-spin Mn$^{2+}$ and Fe$^{2+}$ complexes showed no d−d bands, which is typical for ligands of this type, and the same behavior is observed for Mn(**Me$_2$EBC**)Cl$_2$ and Fe(**Me$_2$EBC**)Cl$_2$.[1] Fe(**Me$_2$EBC**)Cl$_2$ has a weak shoulder at 350 nm ($\varepsilon$ = 260 M$^{-1}$ cm$^{-1}$) that is not present in the manganese complex. Likewise, there is an additional absorbance for Fe(**PyMeEBC**)Cl$^+$ at 403 nm ($\varepsilon$ = 225 M$^{-1}$ cm$^{-1}$). This band is likely associated with the chloro ligand because the presence of a similar band in Fe(**Me$_2$EBC**)Cl$_2$ is not dependent on the pyridine.

The electronic spectrum of the cobalt complex is similar to those of other high-spin octahedral cobalt(II) complexes, having a single major absorption typically between about 500 and 600 nm. This band is due to the $^4T_{1g}(P) \rightarrow {^4T_{1g}(D)}$ transition.[58] The Co(**PyMeEBC**)Cl$^+$ absorbance is at 499 nm ($\varepsilon$ = 34 M$^{-1}$ cm$^{-1}$), which is similar to the Co(**Me$_2$EBC**)Cl$_2$ complex, which absorbs at 540 nm ($\varepsilon$ = 24 M$^{-1}$ cm$^{-1}$).[51]

Ni(**PyMeEBC**)Cl$^+$ exhibits a classic octahedral Ni$^{2+}$ spectrum with three major absorbances between 300 and 1100 nm in acetonitrile.[58] This spectrum allows us to determine the ligand field strength, which is taken as the

**Table 3. Selected Bond Lengths [Å] and Angles [deg]**

[Mn(**PyMeEBC**)Cl]PF$_6$

| | | | | | | | |
|---|---|---|---|---|---|---|---|
| Mn1−N1 | 2.256(2) | N1−Mn1−N3 | 163.43(11) | N2−Mn1−N4 | 164.74(9) | N1−Mn1−Cl1 | 89.44(7) |
| Mn1−N3 | 2.257(3) | N1−Mn1−N2 | 76.79(9) | N1−Mn1−N5 | 90.39(10) | N3−Mn1−Cl1 | 99.53(7) |
| Mn1−N4 | 2.305(3) | N3−Mn1−N2 | 88.99(10) | N3−Mn1−N5 | 78.40(10) | N2−Mn1−Cl1 | 91.53(7) |
| Mn1−N2 | 2.299(3) | N1−Mn1−N4 | 111.45(9) | N2−Mn1−N5 | 78.91(9) | N4−Mn1−Cl1 | 101.15(7) |
| Mn1−N5 | 2.307(3) | N3−Mn1−N4 | 80.63(10) | N4−Mn1−N5 | 88.01(9) | N5−Mn1−Cl1 | 170.22(7) |
| Mn1−Cl1 | 2.4330(9) | | | | | | |

[Fe(**PyMeEBC**)Cl]PF$_6$

| | | | | | | | |
|---|---|---|---|---|---|---|---|
| Fe1−N3 | 2.204(2) | N3−Fe1−N1 | 167.98(9) | N5−Fe1−N2 | 80.29(8) | N3−Fe1−Cl1 | 98.15(6) |
| Fe1−N1 | 2.215(2) | N3−Fe1−N5 | 80.82(8) | N3−Fe1−N4 | 80.31(9) | N1−Fe1−Cl1 | 88.72(6) |
| Fe1−N5 | 2.232(2) | N1−Fe1−N5 | 90.89(8) | N1−Fe1−N4 | 108.49(8) | N5−Fe1−Cl1 | 171.26(6) |
| Fe1−N2 | 2.246(2) | N3−Fe1−N2 | 92.17(9) | N5−Fe1−N4 | 89.58(8) | N2−Fe1−Cl1 | 91.10(6) |
| Fe1−N4 | 2.285(2) | N1−Fe1−N2 | 77.78(8) | N2−Fe1−N4 | 168.27(8) | N4−Fe1−Cl1 | 98.83(6) |
| Fe1−Cl1 | 2.3805(7) | | | | | | |

[Co(**PyMeEBC**)Cl]PF$_6$

| | | | | | | | |
|---|---|---|---|---|---|---|---|
| Co1−N3 | 2.157(3) | N3−Co1−N5 | 82.88(13) | N1−Co1−N2 | 78.78(12) | N3−Co1−Cl1 | 95.69(10) |
| Co1−N5 | 2.175(3) | N3−Co1−N1 | 171.69(14) | N3−Co1−N4 | 81.55(13) | N5−Co1−Cl1 | 171.36(9) |
| Co1−N1 | 2.177(3) | N5−Co1−N1 | 92.69(13) | N5−Co1−N4 | 91.59(12) | N1−Co1−Cl1 | 87.64(9) |
| Co1−N2 | 2.206(3) | N3−Co1−N2 | 93.59(13) | N1−Co1−N4 | 105.68(12) | N2−Co1−Cl1 | 89.71(9) |
| Co1−N4 | 2.263(3) | N5−Co1−N2 | 81.90(12) | N2−Co1−N4 | 172.34(12) | N4−Co1−Cl1 | 96.63(9) |
| Co1−Cl1 | 2.3989(12) | | | | | | |

[Cu(**PyMeEBC**)](PF$_6$)$_2$

| | | | | | | | |
|---|---|---|---|---|---|---|---|
| Cu1−N2 | 2.046(3) | N2−Cu1−N4 | 175.66(13) | N4−Cu1−N5 | 91.27(13) | N4−Cu1−N3 | 86.85(12) |
| Cu1−N4 | 2.079(3) | N2−Cu1−N1 | 79.27(12) | N1−Cu1−N5 | 146.87(12) | N1−Cu1−N3 | 123.66(12) |
| Cu1−N1 | 2.125(3) | N4−Cu1−N1 | 104.95(12) | N2−Cu1−N3 | 91.64(12) | N5−Cu1−N3 | 85.24(12) |
| Cu1−N5 | 2.135(3) | N2−Cu1−N5 | 84.54(13) | | | | |
| Cu1−N3 | 2.136(3) | | | | | | |

[Ni(**PyMeEBC**)Cl]PF$_6$

| | | | | | | | |
|---|---|---|---|---|---|---|---|
| Ni1−N3 | 2.101(3) | N3−Ni1−N5 | 84.75(11) | N3−Ni1−Cl1 | 94.18(8) | N12−Ni2−N11 | 81.39(14) |
| Ni1−N5 | 2.127(3) | N3−Ni1−N1 | 172.93(12) | N5−Ni1−Cl1 | 174.34(9) | N13−Ni2−N14 | 82.95(12) |
| Ni1−N1 | 2.129(3) | N5−Ni1−N1 | 93.39(12) | N1−Ni1−Cl1 | 87.00(8) | N15−Ni2−N14 | 89.46(11) |
| Ni1−N2 | 2.153(3) | N3−Ni1−N2 | 91.87(12) | N2−Ni1−Cl1 | 90.10(9) | N12−Ni2−N14 | 173.32(11) |
| Ni1−N4 | 2.200(3) | N5−Ni1−N2 | 84.38(12) | N4−Ni1−Cl1 | 95.16(8) | N11−Ni2−N14 | 101.85(12) |
| Ni1−Cl1 | 2.4310(9) | N1−Ni1−N2 | 81.15(12) | N13−Ni2−N15 | 84.95(11) | N13−Ni2−Cl2 | 94.79(8) |
| Ni2−N13 | 2.095(3) | N3−Ni1−N4 | 84.48(12) | N13−Ni2−N12 | 93.68(14) | N15−Ni2−Cl2 | 176.45(8) |
| Ni2−N15 | 2.122(3) | N5−Ni1−N4 | 90.28(12) | N15−Ni2−N12 | 84.49(12) | N12−Ni2−Cl2 | 91.99(9) |
| Ni2−N12 | 2.125(3) | N1−Ni1−N4 | 102.37(12) | N13−Ni2−N11 | 174.96(13) | N11−Ni2−Cl2 | 86.47(8) |
| Ni2−N11 | 2.135(3) | N2−Ni1−N4 | 173.80(11) | N15−Ni2−N11 | 93.49(11) | N14−Ni2−Cl2 | 94.02(8) |
| Ni2−N14 | 2.223(3) | | | | | | |
| Ni2−Cl2 | 2.3923(9) | | | | | | |

[Zn(**PyMeEBC**)Cl]PF$_6$ Form 1

| | | | | | | | |
|---|---|---|---|---|---|---|---|
| Zn1−N3 | 2.157(4) | N3−Zn1−N1 | 168.60(15) | N3−Zn1−Cl1 | 96.48(11) | N12−Zn2−N15 | 81.55(14) |
| Zn1−N1 | 2.182(4) | N3−Zn1−N4 | 83.94(15) | N1−Zn1−Cl1 | 88.61(11) | N13−Zn2−N14 | 83.38(14) |
| Zn1−N4 | 2.221(4) | N1−Zn1−N4 | 105.60(15) | N4−Zn1−Cl1 | 97.19(12) | N11−Zn2−N14 | 104.37(14) |
| Zn1−N5 | 2.222(4) | N3−Zn1−N5 | 81.59(14) | N5−Zn1−Cl1 | 173.70(11) | N12−Zn2−N14 | 169.59(14) |
| Zn1−N2 | 2.225(4) | N1−Zn1−N5 | 92.25(15) | N2−Zn1−Cl1 | 92.42(12) | N15−Zn2−N14 | 88.55(13) |
| Zn1−Cl1 | 2.4123(14) | N4−Zn1−N5 | 88.59(15) | N13−Zn2−N11 | 170.23(15) | N13−Zn2−Cl2 | 96.97(10) |
| Zn2−N13 | 2.146(4) | N3−Zn1−N2 | 90.17(15) | N13−Zn2−N12 | 92.06(16) | N11−Zn2−Cl2 | 88.12(10) |
| Zn2−N11 | 2.196(4) | N1−Zn1−N2 | 79.40(14) | N11−Zn2−N12 | 79.30(15) | N12−Zn2−Cl2 | 93.06(11) |
| Zn2−N12 | 2.210(4) | N4−Zn1−N2 | 169.23(15) | N13−Zn2−N15 | 82.17(14) | N15−Zn2−Cl2 | 174.49(10) |
| Zn2−N15 | 2.222(3) | N5−Zn1−N2 | 81.62(15) | N11−Zn2−N15 | 91.96(14) | N14−Zn2−Cl2 | 96.77(10) |
| Zn2−N14 | 2.229(4) | | | | | | |
| Zn2−Cl2 | 2.3818(12) | | | | | | |

[Zn(**PyMeEBC**)Cl]PF$_6$ Form 2

| | | | | | | | |
|---|---|---|---|---|---|---|---|
| Zn1−N3 | 2.163(3) | N3−Zn1−N1 | 167.98(12) | N2−Zn1−N5 | 81.26(11) | N3−Zn1−Cl1 | 97.38(8) |
| Zn1−N4 | 2.256(3) | N3−Zn1−N2 | 89.81(11) | N3−Zn1−N4 | 83.32(11) | N1−Zn1−Cl1 | 89.60(8) |
| Zn1−N5 | 2.249(3) | N1−Zn1−N2 | 79.94(11) | N1−Zn1−N4 | 105.49(11) | N2−Zn1−Cl1 | 93.77(8) |
| Zn1−N2 | 2.210(3) | N3−Zn1−N5 | 81.76(11) | N2−Zn1−N4 | 167.17(11) | N5−Zn1−Cl1 | 174.94(8) |
| Zn1−N1 | 2.183(3) | N1−Zn1−N5 | 90.42(10) | N5−Zn1−N4 | 87.02(11) | N4−Zn1−Cl1 | 97.84(8) |
| Zn1−Cl1 | 2.4043(10) | | | | | | |

**Table 4. Electronic Spectra of M(PyMeEBC) Complexes in Acetonitrile**

| complex | ligand-based and charge-transfer bands, nm ($\varepsilon$, $M^{-1}$ $cm^{-1}$) | d−d bands, nm ($\varepsilon$, $M^{-1}$ $cm^{-1}$) |
|---|---|---|
| Zn(**PyMeEBC**)Cl$^+$ | 317 (220), 264 (4120) | |
| Mn(**PyMeEBC**)Cl$^+$ | 322 (266), 263 (4460) | |
| Fe(**PyMeEBC**)Cl$^+$ | 403 (225), 317 (230), 263 (4550) | |
| Co(**PyMeEBC**)Cl$^+$ | 323 (650), 259 (8150) | 499 (34) |
| Ni(**PyMeEBC**)Cl$^+$ | 310 (177), 264 (3730) | 891 (13), 551sh (19), 422sh (42) |
| Cu(**PyMeEBC**)$^{2+}$ | 286 (5240), 264 (7430) | 639 (101), 1042 (42) |

energy of the lowest-energy absorption band.[59] In this case, the absorption at 891 nm ($\varepsilon = 13$ $M^{-1}$ $cm^{-1}$) converts to $\Delta_0 = 11223$ $cm^{-1}$. In comparison, Ni(**Me$_2$EBC**)Cl$_2$ gave $\Delta_0 = 10215$ $cm^{-1}$ from a similar calculation. Clearly, the pendant pyridine donor increases the ligand field strength, as might be expected for replacement of one chloro ligand by a pyridine. Yet, as shown by the magnetic moment data above, all of the complexes remain high spin.

The Cu(**PyMeEBC**)$^{2+}$ complex exhibits the expected Cu$^{2+}$ d$^9$ d−d band at 639 nm ($\varepsilon = 101$ $M^{-1}$ $cm^{-1}$). This compares to the analogous absorption at 671 nm ($\varepsilon = 100$ $M^{-1}$ $cm^{-1}$) for Cu(**Me$_2$EBC**)Cl$^+$.[39] Interestingly, Cu(**PyMeEBC**)$^{2+}$ has an additional broad peak stretching from 830 to 1200 nm, with its maximum at 1042 nm ($\varepsilon = 42$ $M^{-1}$ $cm^{-1}$), which is not normally observed for this ion. Cu$^{2+}$ complexes typically have only a single absorbance in the visible region representing up to three different unresolved transitions.[58] However, trigonal and tetragonal distortions can lead to one higher-intensity band in the visible range and one lower-intensity band in the near-IR.[58] The exact nature of the distortion is difficult to assign based on the spectrum alone. Fortunately, the obtained X-ray crystal structure confirms a tetragonally distorted 5-coordinate structure for Cu(**PyMeEBC**)$^{2+}$ that may give rise to its electronic spectrum.

**Electrochemical Studies.** In selecting **PyMeEBC** as a target for the development of oxidation catalysts based on **Me$_2$EBC**, we expected the addition of the pyridine donor to lead to changes in the electrochemistry of the resulting complexes. Table 5 shows the potential and peak separation for the Mn−Cu complexes of both of these ligands. Figure 6 shows the cyclic voltammograms of all **PyMeEBC** complexes. Three main trends can be observed in examining this data. The two manganese complexes, Mn(**PyMeEBC**)Cl$^+$ and Mn-(**Me$_2$EBC**)Cl$_2$, will be used to illustrate the trends, which generally hold for all five metals (Mn−Cu) examined.

(1) Oxidation is significantly more positive for the **PyMeEBC** complexes. The Mn$^{2+}$/Mn$^{3+}$ redox couple is at +0.812 V for the **PyMeEBC** complex, while this value is +0.585 V for the **Me$_2$EBC** complex. Similarly, the Mn$^{3+}$/Mn$^{4+}$ couples are at +1.744 and +1.343 V for **PyMeEBC** and **Me$_2$EBC**, respectively. A simple explanation for this behavior is the replacement of a negatively charged chloro ligand with a neutral pyridine donor in **PyMeEBC**. The two negatively charged chloro ligands in the **Me$_2$EBC** complexes clearly favor oxidation compared to the single chloro and pyridine donor in **PyMeEBC**. Access to stable species at higher oxidation potentials may allow oxidation processes with more difficult-to-

**Table 5. Redox Potentials (vs SHE) with Peak Separations for PyMeEBC and Me$_2$EBC Complexes$^a$**

| complex | redox process | potential (V) | peak separation (mV) | ref |
|---|---|---|---|---|
| Mn(**PyMeEBC**)Cl$^+$ | Mn$^+$/Mn$^{2+}$ | $E_{1/2} = -0.526$ | 246 | |
| | Mn$^{2+}$/Mn$^{3+}$ | $E_{1/2} = +0.812$ | 74 | |
| | Mn$^{3+}$/Mn$^{4+}$ | $E_{1/2} = +1.744$ | 286 | |
| Mn(**Me$_2$EBC**)Cl$_2$ | Mn$^{2+}$/Mn$^{3+}$ | $E_{1/2} = +0.585$ | 61 | 1 |
| | Mn$^{3+}$/Mn$^{4+}$ | $E_{1/2} = +1.343$ | 65 | 1 |
| Fe(**PyMeEBC**)Cl$^+$ | Fe$^+$/Fe$^{2+}$ | $E_{1/2} = -1.969$ | 126 | |
| | Fe$^{2+}$/Fe$^{3+}$ | $E_{1/2} = +0.563$ | 82 | |
| Fe(**Me$_2$EBC**)Cl$_2$ | Fe$^{2+}$/Fe$^{3+}$ | $E_{1/2} = +0.110$ | 63 | 1 |
| Co(**PyMeEBC**)Cl$^+$ | Co$^+$/Co$^{2+}$ | $E_{1/2} = -1.386$ | 143 | |
| | Co$^+ \rightarrow$ Co$^{2+}$ | $E_{ox} = -1.200$ | | |
| | Co$^{2+}$/Co$^{3+}$ | $E_{1/2} = +0.657$ | 154 | |
| Co(**Me$_2$EBC**)Cl$_2$ | Co$^{2+} \rightarrow$ Co$^+$ | $E_{red} = -2.198$ | | 51 |
| | Co$^{2+}$/Co$^{3+}$ | $E_{1/2} = +0.173$ | 103 | 51 |
| Ni(**PyMeEBC**)Cl$^+$ | Ni$^{2+} \rightarrow$ Ni$^+$ | $E_{red} = -1.026$ | | |
| | Ni$^{2+} \rightarrow$ Ni$^{3+}$ | $E_{ox} = +1.290$ | | |
| Ni(**Me$_2$EBC**)Cl$_2$ | Ni$^{2+} \rightarrow$ Ni$^+$ | $E_{red} = -1.894$ | | 56 |
| | Ni$^{2+}$/Ni$^{3+}$ | $E_{1/2} = +0.991$ | 154 | 56 |
| Cu(**PyMeEBC**)$^{2+}$ | Cu$^+$/Cu$^{2+}$ | $E_{1/2} = -0.402$ | 80 | |
| Cu(**Me$_2$EBC**)Cl$^+$ | Cu$^{2+} \rightarrow$ Cu$^+$ | $E_{red} = -0.544$ | | 60 |
| | Cu$^{2+} \rightarrow$ Cu$^{3+}$ | $E_{ox} = +1.530$ | | 60 |

$^a$If no reference is listed, the data are from this work.
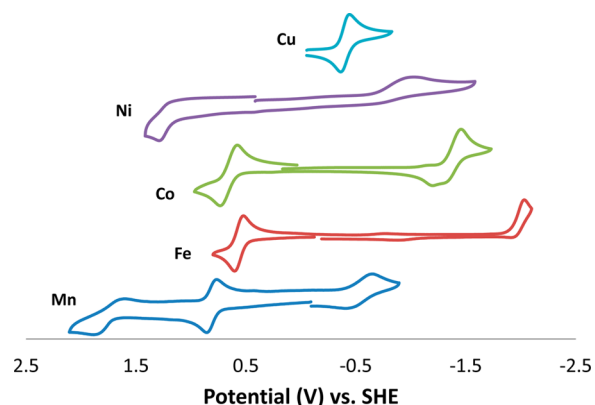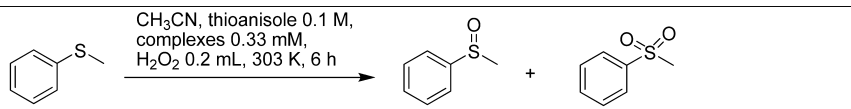


**Figure 6.** Cyclic voltammograms for Cu(**PyMeEBC**)$^{2+}$, Ni-(**PyMeEBC**)Cl$^+$, Co(**PyMeEBC**)Cl$^+$, Fe(**PyMeEBC**)Cl$^+$, and Mn-(**PyMeEBC**)Cl$^+$.
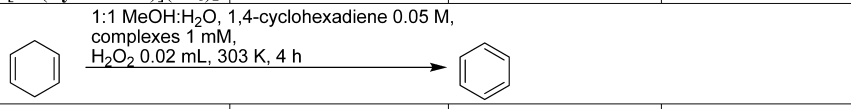
oxidize substrates if this property is present in catalytically active species of the **PyMeEBC** complexes.

(2) Reduction is significantly easier for the **PyMeEBC** complexes. One less negatively charged chloro ligand allows reversible reduction to occur in acetonitrile for the manganese complex of **PyMeEBC** (at −0.526 V), whereas this reduction is not observed at all for the manganese complex of **Me$_2$EBC**.

(3) A general trend toward reversible access to a larger range of oxidation states is observed in most cases for the **PyMeEBC**

**Table 6. Oxidation Catalysis Screening Results for Mn$^{II}$, Fe$^{II}$, and Cu$^{II}$ Complexes of PyMeEBC in Comparison to Mn(Me$_2$EBC)Cl$_2$**



CH$_3$CN, thioanisole 0.1 M, complexes 0.33 mM, H$_2$O$_2$ 0.2 mL, 303 K, 6 h

| Complex | Conversion % | Yield % Sulfoxide | Yield % Sulfone |
|---|---|---|---|
| Mn(**Me$_2$EBC**)Cl$_2$ | 99.8 | 44.3 | 46.5 |
| [Mn(**PyMeEBC**)Cl]Cl | 75.3 | 53.9 | 14.1 |
| [Fe(**PyMeEBC**)Cl]PF$_6$ | 47.2 | 30.1 | 12.5 |
| [Cu(**PyMeEBC**)](PF$_6$)$_2$ | 11.7 | 9.2 | 0.71 |

1:1 MeOH:H$_2$O, 1,4-cyclohexadiene 0.05 M, complexes 1 mM, H$_2$O$_2$ 0.02 mL, 303 K, 4 h

| Complex | Conversion % | Yield % Benzene | |
|---|---|---|---|
| Mn(**Me$_2$EBC**)Cl$_2$ | 86.2 | 71.4 | |
| [Mn(**PyMeEBC**)Cl]Cl | 88.0 | 51.2 | |
| [Fe(**PyMeEBC**)Cl]PF$_6$ | 55.3 | 33.3 | |
| [Cu(**PyMeEBC**)](PF$_6$)$_2$ | 23.2 | 3.7 | |

ligand (see Figure 6). Reversible access to Mn$^+$/Mn$^{2+}$/Mn$^{3+}$/Mn$^{4+}$, Fe$^+$/Fe$^{2+}$/Fe$^{3+}$, Co$^+$/Co$^{2+}$/Co$^{3+}$, and Cu$^+$/Cu$^{2+}$ is observed for the **PyMeEBC** complexes, whereas reversible access for **Me$_2$EBC** complexes is restricted to Mn$^{2+}$/Mn$^{3+}$/Mn$^{4+}$, Fe$^{2+}$/Fe$^{3+}$, Co$^{2+}$/Co$^{3+}$, and only Cu$^{2+}$. Catalytic processes would require reversible access to multiple oxidation states, although the utility for oxidation catalysis of reversibly accessing the M$^+$ oxidation states in the **PyMeEBC** complexes is not obvious.

Interestingly, neither oxidation to Ni$^{3+}$ nor reduction to Ni$^+$ is reversible for Ni(**PyMeEBC**)Cl$^+$, even though the Ni$^{2+}$/Ni$^{3+}$ redox couple is reversible for Ni(**Me$_2$EBC**)Cl$_2$. Perhaps two chloro ligands are required to stabilize the Ni$^{3+}$ ion, while only one is present in Ni(**PyMeEBC**)Cl$^+$. Similarly, the lack of even one chloro ligand in Cu(**PyMeEBC**)$^{2+}$ eliminates the oxidation to Cu$^{3+}$ altogether, even though a nonreversible oxidation to Cu$^{3+}$ is observed (+1.530 V) for Cu(**Me$_2$EBC**)Cl$^+$. However, the Cu$^+$/Cu$^{2+}$ redox process is reversible for Cu(**PyMeEBC**)$^{2+}$, although nonreversible for Cu(**Me$_2$EBC**)Cl$^+$. In the latter complex, loss of the chloro ligand upon reduction to Cu$^+$ is reasonable and is supported by a related 4-coordinate copper(I) complex crystal structure.[61] Loss of the fifth (pyridine) donor is not likely for Cu(**PyMeEBC**)$^{2+}$ because the pyridine donor is neutral and, probably more important, because it is covalently bound to the rest of the ligand.

**Catalytic Oxidation Screening.** Screening for the oxidation reactivity of the biologically relevant manganese, iron, and copper complexes in catalytic processes may not only help to understand the behaviors of related metalloenzymes but also guide the exploration of these complexes' potential applications. In the electrochemical studies above, it has been observed that **PyMeEBC**-ligated metal ions demonstrate reversible redox behaviors, which provides the basis to explore their catalytic activity in oxidations.

**HAT.** The catalytic oxidation properties of the Mn$^{2+}$, Fe$^{2+}$, and Cu$^{2+}$ complexes were first investigated in HAT (Table 6), which is the most fundamental process in redox chemistry.[62] Using 1,4-cyclohexadiene as the substrate with H$_2$O$_2$ oxidant, after reaction at 303 K for 4 h in acetonitrile, the Mn$^{II}$ complex of **PyMeEBC** produces 51.2% yield of benzene with 88.0% conversion, while the corresponding Fe$^{II}$ complex yields only 33.3% of benzene with 55.3% conversion. Because these two complexes are isostructural (vide supra), these functional

differences clearly have electronic/electrochemical rather than structural origins. The higher oxidation potential of the Mn$^{2+/3+}$ couple compared to the Fe$^{2+/3+}$ couple and access to Mn$^{4+}$ while Fe$^{4+}$ is not available, as discussed in the Electrochemistry section, likely explains the more efficient HAT.
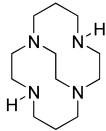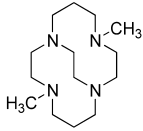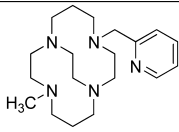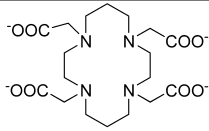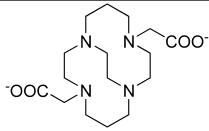
Compared with the high conversion, the relatively low yield of benzene with the Mn$^{II}$ complex **PyMeEBC** is possibly related to its OAT activity, which leads to the formation of epoxide (vide infra), but the products were not identified in GC analysis. In comparison, the Mn$^{II}$ complex with the **Me$_2$EBC** ligand is much more active and gives 71.4% yield of benzene with 86.2% conversion. A multitude of other synthetic manganese complexes have shown excellent catalytic HAT ability, so this is not unique or unexpected. However, it is reassuring that the addition of a fifth donor atom to the cross-bridged cyclam chelate has not eliminated this reactivity for Mn(**PyMeEBC**), and future studies will aim at elucidating the mechanism of HAT by Mn(**PyMeEBC**).

The Cu$^{II}$ complex of **PyMeEBC** is very sluggish as a catalyst for HAT: the yield of benzene is close to its natural content in commercial 1,4-cyclohexadiene (~3%). The lack of reactivity of the copper complex is most logically explained not by its structure, which is, in fact, different from the isostructural iron and manganese complexes yet retains the entire 5-coordinate **PyMeEBC** ligand, but rather its electrochemistry, which lacks any oxidation states above Cu$^{2+}$ and suggests that this is just not reactive enough to result in substrate oxidation.

**OAT.** For OAT screening, thioanisole was selected as the substrate and acetonitrile was employed as the solvent with H$_2$O$_2$ oxidant. After reaction at 303 K for 6 h, the Mn$^{II}$ complex **PyMeEBC** gives 53.9% yield of sulfoxide with 14.1% of sulfone, while the conversion is 75.3%. The Fe$^{II}$ complex gives 30.1% of sulfoxide and 12.5% of sulfone with 47.2% conversion. Similar to the HAT experiment, the Cu$^{II}$ complex is inactive for sulfide oxidation, with results comparable to those from the control experiment without catalyst.

Again, Mn(**Me$_2$EBC**) is more active in sulfide oxidation, yielding 44.3% of sulfoxide and 46.5% of sulfone with almost complete conversion of sulfide. In comparison, Mn-(**PyMeEBC**) only produces 14.1% of sulfone, with most of its product (53.9%) the sulfoxide and only 75.3% conversion. It appears that the addition of the 2-pyridylmethyl pendant arm lowered the overall reactivity (less conversion and less sulfone)

**Table 7. Half-lives of Selected Cu$^{II}$ Complexes in 5 M HCl**

| Complex | 50 °C | 90 °C | reference | Ligand Structure |
|---|---|---|---|---|
| Cu(**H₂EBC**) | ----- | 11.8 min | [71] | |
| Cu(**Me₂EBC**) | 7.3 d | 79 min | this work | |
| Cu(**PyMeEBC**) | 14.7 min | < 2 min | this work | |
| Cu(**TETA**) | 3.2 hour | 4.5 min | [71] | |
| Cu(**CB-TE2A**) | ----- | 154 hour | [71] | |

but improved the selectivity for the sulfoxide product. As shown in Table 5, the redox potential of the Mn$^{3+}$/Mn$^{4+}$ couple for Mn(**Me₂EBC**)Cl$_2$ is substantially lower than that for Mn(**PyMeEBC**)Cl$^+$ (+1.343 vs +1.744 V). Also, the peak separation shows that Mn(**Me₂EBC**)Cl$_2$ is electrochemically reversible, while the reversibility is not so good for Mn-(**PyMeEBC**)Cl$^+$. Clearly, oxidizing Mn(**PyMeEBC**)Cl$^+$ to the corresponding Mn$^{IV}$ complex is not as easy as Mn(**Me₂EBC**)-Cl$_2$, where the Mn$^{IV}$ complex can be obtained in large scale, and this may explain its relatively poor efficiency in sulfide oxygenation in which the Mn$^{IV}$ species may play a significant role.[12]

In terms of utility, this selectivity for sulfoxide production may be advantageous. Organic sulfoxides are useful synthetically for the production of pharmaceuticals and other valuable chemical compounds.[63,64] A number of synthetic manganese catalysts have been developed that can efficiently transform sulfides into sulfoxides and/or sulfones.[64−69] The closest literature analogues to Mn(**Me₂EBC**) and Mn(**PyMeEBC**) are probably the manganese complexes of 1,4,7-trimethyl-1,4,7-triazacyclononane (**TMTACN**),[67−69] which generally demonstrate a more efficient sulfide oxygenation activity. In this catalyst, a manganese(V) oxo intermediate was proposed to serve as the oxygenation species by a concerted OAT or electron-transfer mechanism, leading to sulfoxide and then sulfone products in two oxidation steps. The Mn(**TMTACN**) catalysts were developed as bleach catalysts for the laundry industry and were actually introduced into consumer products. Yet, their lack of selectivity in oxidation reactivity contributed to their removal from those consumer products because of their

damage to cloth.[69] Although Mn(**PyMeEBC**) does not appear to be as highly efficient as some of these other catalysts based on the above initial screening data, we look forward to future studies aimed at fully understanding its oxidation mechanisms and attempting to optimize its sulfoxidation selectivity.

Although these catalytic oxidations are very preliminary, with further mechanistic elucidation the subject of future work, they have provided useful information regarding the potential applications of these metal complexes with the **PyMeEBC** ligand. Another potential application with selective mild oxidation, in addition to the formation of sulfoxides rather than sulfones, is the laundry industry. Here, a good catalyst should be efficient enough to oxygenate the soil for its removal from clothes but must be sluggish enough in HAT to avoid damage to cotton or other textiles.[16−20] The Mn$^{II}$ complex with **Me₂EBC** has demonstrated its ability to serve as a redox catalyst in detergent but has not yet been embraced by the industry, perhaps because it is too reactive.[16−20] Here, the Mn$^{II}$ complex with **PyMeEBC** seems to be even more attractive as a detergent catalyst because it has an oxygenation efficiency comparable to that of the Mn(**Me₂EBC**)$^{2+}$ complex, while its HAT power is desirably more sluggish. More detailed studies on this issue are still in progress to explore the potentially useful redox chemistry of **PyMeEBC** complexes.

**Kinetic Stability.** A particularly useful property of cross-bridged tetraazamacroycle complexes, because of their topological complexity and rigidity caused by their small size, is their typically extreme stability under harsh conditions.[1−4] As established by Busch et al.[1,70] and standardized by Weisman et al.,[71−74] probing the stability of new cross-bridged ligands is

now routinely done using the Cu$^{II}$ complex, which is often the first (or only) transition-metal complex synthesized because of the interest in positron emission tomography (PET) imaging applications of $^{64}$Cu. Weisman et al. have chosen 5 M HCl and various temperature points, such as 30, 50, and 90 °C, as benchmarks for the kinetic stability of new copper cross-bridged complexes. Unfortunately, the proton-sponge nature of these ligands prevents aqueous titration in the presence of a metal ion to yield formation constants because the ligand never gives up its last proton(s) and the complex is not formed. Instead, kinetic decomplexation studies in the presence of high acid concentration under pseudo-first-order conditions are used to give some measure of complex stability. Currently, only Cu$^{II}$ complexes have undergone these studies and yielded published data for comparison.

Although Cu(**Me$_2$EBC**)Cl$^+$ was the first cross-bridged complex to undergo this sort of experiment,[50] the 1 M HClO$_4$ and 40 °C conditions used make comparison to Weisman's database of compounds difficult. We have, therefore, resynthesized this complex and tested it, as well as Cu-(**PyMeEBC**)$^{2+}$, in order to determine the effects of adding the 2-pyridylmethyl pendant arm to the ethylene cross-bridged ligand. The results of the decomplexation studies are presented in Table 7, along with relevant literature data for comparison.

According to the teachings of coordination chemistry,[75] if we add additional chelate rings, a polydentate ligand typically forms *more* stable transition-metal complexes, as long as the metal−ligand match in size, geometry, and electronics is not perturbed. For example, Weisman et al.'s bis(carboxylate) pendant-armed cross-bridged ligand **CB-TE2A** (Table 7) gains up to 4 orders of magnitude in stability versus the **H$_2$EBC** complex, as seen in Table 7. In contrast, the stability of the Cu$^{II}$ complex decreases, from a 79 min half-life for tetradentate **Me$_2$EBC** at 90 °C in 5 M HCl to less than 2 min for pentadentate **PyMeEBC**, even though an additional chelate ring involving the pyridine pendant arm has been added to the structure. A similar, and more easily measurable, decrease in the stability was observed at 50 °C from 7.3 days to 14.7 min.

This appears to be the first example of subtraction of stability upon the addition of chelating groups to a cross-bridged tetraazamacrocycle parent structure. Perhaps the strain noted for the four-membered chelate rings involving the pyridine donors [N2−Cu1−N1 = 79.27(12)°] in the discussion of the X-ray crystal structures above reveals that the geometry match between metal and ligand is disrupted by the pyridine pendant arm, making dissociation easier. Weisman's Cu(**CB-TE2A**) can actually protonate one of the acetate pendant arms without dissociating either chelate arm, likely a key to its acid stability. Perhaps telling is that the chelate bond angle for the O−Cu−N chelate ring of the acetate pendant arm that does not protonate is much less strained at 84.03(7)°, according to a crystal structure of the monoprotonated complex.[71] Whatever the mechanism, the addition of the pyridine pendant arm clearly destabilizes its Cu$^{II}$ complex toward acid decomplexation compared to other cross-bridged cyclam ligands, and even the unbridged ligand **TETA** is more stable toward decomplexation under the same conditions (Table 7).

Interestingly, the Cu$^{2+}$ complex of a bis(2-pyridylmethyl) pendant-armed cross-bridged cyclen (**CRpy$_2$**; Figure 7) ligand is, in fact, stabilized toward acid decomplexation compared to its dimethyl analogue (**Me$_2$Bcyclen**).[36] In this case, **CRpy$_2$** is lost at 25 °C in 3 M HClO$_4$ with an estimated half-life of 7 days, while the dimethyl ligand is lost from Cu$^{2+}$ at 25 °C in 1
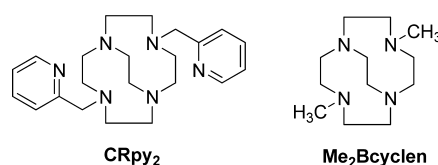


**Figure 7.** Cross-bridged cyclen ligands discussed.

M HClO$_4$ with a half-life of 30 h.[60] No crystal structure of the Cu(**CRpy$_2$**) ligand was obtained, so strain arguments cannot be used in this case. Why one pyridine pendant arm destabilizes a given copper complex while two pyridine pendant arms stabilize another is a compelling problem.

Even though its copper complex is destabilized toward strong acid decomplexation, the Cu$^{II}$, Fe$^{II}$, and Mn$^{II}$ complexes of **PyMeEBC** gave no visual signs of decomplexation during the oxidation catalysis screening reactions discussed above. Manganese and iron complexes typically give insoluble oxide precipitates under oxidizing conditions, such as the H$_2$O$_2$ conditions used in the oxidation reactions tested. No precipitates were observed during these reactions, qualitatively indicating sufficient stability under the conditions used. Additional stability experiments for these complexes will accompany the mechanistic experiments planned to fully understand their redox catalysis.

## ■ CONCLUSIONS

A new pyridylmethyl N-pendant-armed cross-bridged cyclam ligand, **PyMeEBC**, has been synthesized with a key synthetic step using nonpolar chloroform as the solvent to reduce the self-reactivity of picolyl chloride in the presence of the cyclam−glyoxal nucleophile. Divalent manganese, iron, cobalt, nickel, copper, and zinc complexes were synthesized and structurally characterized by X-ray crystallography. **PyMeEBC** binds each metal ion in a cis-V configuration of the cyclam ring, with the chelated pyridine nitrogen bound to each metal ion and a chloro ligand occupying the sixth coordination site in all but the 5-coordinate Cu$^{2+}$ complex. Solid-state magnetic moment and acetonitrile solution electronic spectroscopy experiments revealed high-spin, octahedral, divalent metal complexes in all cases, again with the exception of the 5-coordinate Cu$^{2+}$ complex. Electrochemical studies under an inert atmosphere and in acetonitrile revealed reversible access to multiple oxidation states, a prerequisite for successful oxidation catalysis, in most cases. In particular, Mn(**PyMeEBC**)Cl$^+$ was stabilized in Mn$^+$/Mn$^{2+}$/Mn$^{3+}$/Mn$^{4+}$ oxidation states. Finally, preliminary screens for oxidation catalysis using H$_2$O$_2$ as the oxidant were carried out on the biomimetically important manganese, iron, and copper complexes and showed promising results, particularly for Mn(**PyMeEBC**)Cl$^+$, in the oxidation of thianisole and HAT of 1,4-cyclohexadiene. Importantly, Mn(**PyMeEBC**)Cl$^+$ demonstrates powerful, yet selective oxidation reactivity that may lead to improved applications where the Mn(**Me$_2$EBC**)Cl$_2$ catalyst may be too reactive, such as in laundry bleaching. Surprisingly, the Cu$^{II}$ complex is actually destabilized toward acid decomplexation by the addition of the pyridine pendant arm compared to the parent **Me$_2$EBC** complex, which may be a result of a strained structure. Future work will include expanding the range of oxidation reactions possible with this catalyst and determination of its oxidation catalysis mechanisms.

## ■ ASSOCIATED CONTENT

### ⒮ Supporting Information

X-ray crystallographic data in CIF format and detailed crystallographic data. This material is available free of charge via the Internet at http://pubs.acs.org.

## ■ AUTHOR INFORMATION

### Corresponding Authors
*E-mail: T.Prior@hull.ac.uk.
*E-mail: gyin@hust.edu.cn.
*E-mail: tim.hubin@swosu.edu.

### Notes
The authors declare no competing financial interest.

## ■ ACKNOWLEDGMENTS

## ■ REFERENCES

(1) Hubin, T. J.; McCormick, J. M.; Collinson, S. R.; Buchalova, M.; Perkins, C. M.; Alcock, N. W.; Kahol, P. K.; Raghunathan, A.; Busch, D. H. *J. Am. Chem. Soc.* **2000**, *122*, 2512−2522.

(2) Hubin, T. J.; McCormick, J. M.; Alcock, N. W.; Busch, D. H. *Inorg. Chem.* **2001**, *40*, 435−444.

(3) Hubin, T. J.; McCormick, J. M.; Collinson, S. R.; Alcock, N. W.; Clase, H. J.; Busch, D. H. *Inorg. Chim. Acta* **2003**, *346*, 76−86.

(4) Hubin, T. J. *Coord. Chem. Rev.* **2003**, *241*, 27−46.

(5) Yin, G.; Buchalova, M.; Danby, A. M.; Perkins, C. M.; Kitko, D.; Carter, J. D.; Scheper, W. M.; Busch, D. H. *J. Am. Chem. Soc.* **2005**, *127*, 17170−17171.

(6) Yin, G.; Danby, A. M.; Kitko, D.; Carter, J. D.; Scheper, W. M.; Busch, D. H. *Inorg. Chem.* **2007**, *46*, 2173−2180.

(7) Yin, G.; Danby, A. M.; Kitko, D.; Carter, J. D.; Scheper, W. M.; Busch, D. H. *J. Am. Chem. Soc.* **2008**, *130*, 16245−16253.

(8) Chattopadhyay, S.; Geiger, R. A.; Yin, G.; Busch, D. H.; Jackson, T. A. *Inorg. Chem.* **2010**, *49*, 7530−7535.

(9) Shi, S.; Wang, Y.; Xu, A.; Wang, H.; Zhu, D.; Roy, S. B.; Jackson, T. A.; Busch, D. H.; Yin, G. *Angew. Chem., Int. Ed.* **2011**, *50*, 7321−7324.

(10) Wang, Y.; Shi, S.; Wang, H.; Zhu, D.; Yin, G. *Chem. Commun.* **2012**, *48*, 7832−7834.

(11) Wang, Y.; Sheng, J.; Shi, S.; Zhu, D.; Yin, G. *J. Phys. Chem. C* **2012**, *116*, 13231−13239.

(12) Wang, Y.; Shi, S.; Zhu, D.; Yin, G. *Dalton Trans.* **2012**, *41*, 2612−2619.

(13) Dong, L.; Wang, Y.; Lu, Y.; Chen, Z.; Mei, F.; Xiong, H.; Yin, G. *Inorg. Chem.* **2013**, *52*, 5418−5427.

(14) Yin, G. *Acc. Chem. Res.* **2013**, *46*, 483−492.

(15) Weisman, G. R.; Rogers, M. E.; Wong, E. H.; Jasinski, J. P.; Paight, E. S. *J. Am. Chem. Soc.* **1990**, *112*, 8604−8605.

(16) Busch, D. H.; Collinson, S. R.; Hubin, T. J.; Perkins, C. M.; Labeque, R.; Williams, B. K.; Johnston, J. P.; Kitko, D. J.; Berkett-St. Laurent, J. C. T. R. Bleach Compositions. U.S. Patent 6,218,351, April 17, 2001.

(17) Busch, D. H.; Collinson, S. R.; Hubin, T. J.; Perkins, C. M.; Labeque, R.; Williams, B. K.; Johnston, J. P.; Kitko, D. J.; Berkett-St. Laurent, J. C. T. R.; Burns, M. E. Bleach Compositions. U.S. Patent 6,387,862, May 14, 2002.

(18) Busch, D. H.; Collinson, S. R.; Hubin, T. J.; Perkins, C. M.; Labeque, R.; Williams, B. K.; Johnston, J. P.; Kitko, D. J.; Berkett-St. Laurent, J. C. T. R.; Burns, M. E. Bleach Compositions. U.S. Patent 6,606,015, August 19, 2003.

(19) Busch, D. H.; Collinson, S. R.; Hubin, T. J. Catalysts and methods for catalytic oxidation. U.S. Patent 6,906,189, June 14, 2005.

(20) Busch, D. H.; Collinson, S. R.; Hubin, T. J.; Perkins, C. M.; Labeque, R.; Williams, B. K.; Johnston, J. P.; Kitko, D. J.; Berkett-St. Laurent, J. C. T. R. Bleach Compositions. U.S. Patent 7,125,832, Oct 24, 2006.

(21) Feng, Y.; England, J.; Que, L. J. *ACS Catal.* **2011**, *1*, 1035−1042.

(22) Yin, G.; Danby, A. M.; Day, V.; Roy, S. B.; Carter, J.; Scheper, W. M.; Busch, D. H. *J. Coord. Chem.* **2011**, *64*, 4−17.

(23) Yin, G.; Roy, S. B.; Danby, A. M.; Day, V.; Carter, J.; Scheper, W. M.; Busch, D. H. *J. Incl. Phenom. Macrocycl. Chem.* **2011**, *71*, 311−318.

(24) Thibon, A.; England, J.; Martinho, M.; Young, V. G. J.; Frisch, J. R.; Guillot, R.; Girerd, J.-J.; Munck, E.; Que, L. J.; Banse, F. *Angew. Chem., Int. Ed.* **2008**, *47*, 7064−7067.

(25) Alcock, N. W.; Balakrishnan, K. P.; Moore, P. *J. Chem. Soc., Dalton Trans.* **1986**, 1743−1745.

(26) Asato, E.; Hashimoto, S.; Matsumoto, N.; Kida, S. *J. Chem. Soc., Dalton Trans.* **1990**, 1741−1746.

(27) Vuckovic, G.; Asato, E.; Matsumoto, N.; Kida, S. *Inorg. Chim. Acta* **1990**, *171*, 45−52.

(28) Royal, G.; Dahaoui-Gindrey, V.; Dahaoui, S.; Tabard, A.; Guilard, R.; Pullumbi, P.; Lecomte, C. *Eur. J. Org. Chem.* **1998**, 1971−1975.

(29) Bucher, C.; Royal, G.; Barbe, J.-M.; Guilard, R. *Tetrahedron Lett.* **1999**, *40*, 2315−2318.

(30) Goeta, A. E.; Howard, J. A. K.; Maffeo, D.; Puschmann, H.; Williams, J. A. G.; Yufit, D. S. *J. Chem. Soc., Dalton Trans.* **2000**, 1873−1880.

(31) Batsanov, A. S.; Goeta, A. E.; Howard, J. A. K.; Maffeo, D.; Puschmann, H.; Williams, J. A. G. *Polyhedron* **2001**, *20*, 981−986.

(32) El Ghachtouli, S.; Cadiou, C.; Dechamps-Olivier, I.; Chuburu, F.; Aplincourt, M.; Roisnel, T. *Eur. J. Inorg. Chem.* **2006**, 3472−3481.

(33) El Ghachtouli, S.; Cadiou, C.; Dechamps-Olivier, I.; Chuburu, F.; Aplincourt, M.; Patinec, V.; Le Baccon, M.; Handel, H.; Roisnel, T. *New J. Chem.* **2006**, *30*, 392−398.

(34) Narayanan, J.; Solano-Peralta, A.; Ugalde-Salvidar, V. M.; Escudero, R.; Hopfl, H.; Sosa-Torres, M. E. *Inorg. Chim. Acta* **2008**, *361*, 2747−2758.

(35) Morfin, J.-F.; Tripier, R.; Le Baccon, M.; Handel, H. *Polyhedron* **2009**, *28*, 3691−3698.

(36) Bernier, N.; Costa, J.; Delgado, R.; Felix, V.; Royal, G.; Tripier, R. *Dalton Trans.* **2011**, *40*, 4514−4526.

(37) Barefield, E. K.; Wagner, F.; Herlinger, A. W.; Dahl, A. R. *Inorg. Synth.* **1976**, *XVI*, 220−225.

(38) Le Baccon, M.; Chuburu, F.; Toupet, L.; Handel, H.; Soibinet, M.; Deschamps-Olivier, I.; Barbier, J.-P.; Aplincourt, M. *New J. Chem.* **2001**, *25*, 1168−1174.

(39) Hubin, T. J.; McCormick, J. M.; Alcock, N. W.; Clase, H. J.; Busch, D. H. *Inorg. Chem.* **1999**, *38*, 4435−4446.

(40) *X-AREA*, version 1.64; Stoe & Cie GmbH: Darmstadt, Germany, 2012.

(41) Sheldrick, G. *Acta Crystallogr., Sect. A: Found. Crystallogr.* **2008**, *64*, 112−122.

(42) Weisman, G. R.; Wong, E. H.; Hill, D. C.; Rogers, M. E.; Reed, D. P.; Calabrese, J. C. *Chem. Commun.* **1996**, 947−948.

(43) Wong, E. H.; Weisman, G. R.; Hill, D. C.; Reed, D. P.; Rogers, M. E.; Condon, J. P.; Fagan, M. A.; Calabrese, J. C.; Lam, K.-C.; Guzei, I. A.; Rheingold, A. L. *J. Am. Chem. Soc.* **2000**, *122*, 10561−10572.

(44) Almassio, M. F.; Sarimbalis, M. N.; Garay, R. O. *Des. Monomers Polym.* **2005**, *8*, 287−296.

(45) Rojas-Limas, S.; Farfan, N.; Santillan, R.; Castillo, D.; Sosa-Torres, M. E.; Hopfl, H. *Tetrahedron* **2000**, *56*, 6427−6433.

(46) El Hajj, F.; Sebki, G.; Patinec, V.; Marchivie, M.; Triki, S.; Handel, H.; Yefsah, S.; Tripier, R.; Gomez-Garcia, C. J.; Coronado, E. *Inorg. Chem.* **2009**, *48*, 10416−10423.

(47) Fuzerova, S.; Kotek, J.; Cisarova, I.; Hermann, P.; Binnemans, K.; Lukes, I. *Dalton Trans.* **2005**, 2908−2915.

(48) Kotek, J. L. P.; Hermann, P.; Cisarova, I.; Lukes, I.; Godula, T.; Svobodova, I.; Taborsky, P.; Havel, J. *Chem.—Eur. J.* **2003**, *9*, 233−248.

(49) Sun, X.; Wuest, M.; Kovacs, Z.; Sherry, A. D.; Motekaitis, R.; Wang, Z.; Martell, A. E.; Welch, M. J.; Anderson, C. J. *J. Biol. Inorg. Chem.* **2003**, *8*, 217−225.

(50) Svobodova, I.; Havlickova, J.; Plutnar, J.; Plutnar, J.; Lubal, P.; Kotek, J.; Hermann, P. *Eur. J. Inorg. Chem.* **2009**, 3577−3592.

(51) Hubin, T. J.; Alcock, N. W.; Clase, H. J.; Seib, L. L.; Busch, D. H. *Inorg. Chim. Acta* **2002**, *337*, 91−102.

(52) Addison, A. W.; Rao, T. N.; Reedijk, J.; van Rijn, J.; Verschoor, G. C. *J. Chem. Soc., Dalton Trans.* **1984**, 1349−1356.

(53) Bondi, A. *J. Phys. Chem.* **1964**, *68*, 441−451.

(54) Groom, C. R.; Allen, F. H. *Angew. Chem., Int. Ed.* **2014**, *53*, 662−671.

(55) Hubin, T. J., unpublished data, 2014.

(56) Hubin, T. J.; Alcock, N. W.; Clase, H. J.; Busch, D. H. *Supramol. Chem.* **2001**, *13*, 261−276.

(57) Burger, K. *Coordination Chemistry: Experimental Methods*; Butterworth: London, 1973.

(58) Lever, A. B. P. *Inorganic Electronic Spectroscopy*, 2nd ed.; Elsevier: Amsterdam, The Netherlands, 1984.

(59) Drago, R. S. *Physical Methods for Chemists*, 2nd ed.; Saunders College Publishing−Harcourt Brace Jovanovich: Ft. Worth, TX, 1992.

(60) Hubin, T. J.; Alcock, N. W.; Morton, M. D.; Busch, D. H. *Inorg. Chim. Acta* **2003**, *348*, 33−40.

(61) Hubin, T. J.; Alcock, N. W.; Busch, D. H. *Acta Crystallogr.* **2000**, *C56*, 37−39.

(62) Mayer, J. M. *Acc. Chem. Res.* **1998**, *31*, 441−450.

(63) Carreno, M. C. *Chem. Rev.* **1995**, *95*, 1717−1760.

(64) Ghorbanloo, M.; Jaworska, M.; Paluch, P.; Li, G.-D.; Zhou, L.-J. *Transtion Met. Chem.* **2013**, *38*, 511−521.

(65) Zhou, X.-T.; Ji, H.-B. *Catal. Commun.* **2014**, *53*, 29−32.

(66) So, H.; Park, Y. J.; Cho, K.-B.; Lee, Y.-M.; Seo, M.-S.; Cho, J.; Sarang, R.; Nam, W. *J. Am. Chem. Soc.* **2014**, *136*, 12229−12232.

(67) Brinksma, J.; La Crois, R.; Feringa, B. L.; Donnoli, M. I.; Rosini, C. *Tetrahedron Lett.* **2001**, *42*, 4049−4052.

(68) Shul'pin, G. B.; Suss-Fink, G.; Shul'pina, L. S. *J. Mol. Catal. A* **2001**, *170*, 17−34.

(69) Lindsay Smith, J. R.; Gilbert, B. C.; Mairata i Payeras, A.; Murray, J.; Lowdon, T. R.; Oakes, J.; Pons i Prats, R.; Walton, P. H. *J. Mol. Catal. A* **2006**, *251*, 114−122.

(70) Hubin, T. J.; McCormick, J. M.; Collinson, S. R.; Alcock, N. W.; Busch, D. H. *Chem. Commun.* **1998**, 1675−1676.

(71) Woodin, K. S.; Heroux, K. J.; Boswell, C. A.; Wong, E. H.; Weisman, G. R.; Niu, W.; Tomellini, S. A.; Anderson, C. J.; Zakharov, L. N.; Rheingold, A. L. *Eur. J. Inorg. Chem.* **2005**, *7*, 4829−4833.

(72) Heroux, K. J.; Woodin, K. S.; Tranchemontagne, D. J.; Widger, P. C. B.; Southwick, E.; Wong, E. H.; Weisman, G. R.; Tomellini, S. A.; Wadas, T. J.; Anderson, C. J.; Kassel, S.; Golen, J. A.; Rheingold, A. L. *Dalton Trans.* **2007**, 2150−2162.

(73) Anderson, C. J.; Wadas, T. J.; Wong, E. H.; Weisman, G. R. *Quart. J. Nucl. Med. Mol. Imaging* **2008**, *52*, 185−192.

(74) Odendaal, A. Y.; Fiamengo, A. L.; Ferdani, R.; Wadas, T. J.; Hill, D. C.; Peng, Y.; Heroux, K. J.; Golen, J. A.; Rheingold, A. L.; Anderson, C. J.; Weisman, G. R.; Wong, E. H. *Inorg. Chem.* **2011**, *50*, 3078−3086.

(75) Busch, D. H. *Chem. Rev.* **1993**, *93*, 847−860.